

BEER analysis of Kepler and CoRoT light curves

III. Spectroscopic confirmation of seventy new beaming binaries discovered in CoRoT lightcurves

L. Tal-Or¹, S. Faigler¹, and T. Mazeh¹

School of Physics and Astronomy, Raymond and Beverly Sackler Faculty of Exact Sciences, Tel Aviv University, Tel Aviv, Israel
e-mail: levta1o@post.tau.ac.il

Received ... ; accepted ...

ABSTRACT

Context. The BEER algorithm, introduced by Faigler & Mazeh (2011), searches stellar lightcurves for the BEaming, Ellipsoidal, and Reflection photometric modulations caused by a short-period companion. These three effects are typically of very low amplitude, and can be detected mainly in lightcurves from space-based photometers. Unlike eclipsing binaries, these effects are not limited to edge-on inclinations.

Aims. Applying the algorithm to wide-field photometric surveys like CoRoT and *Kepler* offers an opportunity to better understand statistical properties of short-period binaries. It also widens the window for detecting intrinsically rare systems, like short-period brown-dwarf and massive-planetary companions to main-sequence stars.

Methods. Applying the search to the first five long-run center CoRoT fields, we identified 481 *non-eclipsing* candidates with periodic flux amplitudes of 0.5–87 mmag. Optimizing the Anglo-Australian-Telescope pointing coordinates and the AAOmega fiber-allocations with dedicated softwares, we acquired 6–7 medium-resolution spectra of 281 candidates in a seven-night campaign. Analysis of the red-arm AAOmega spectra, which covered the range of 8342–8842 Å, yielded a radial-velocity precision of ~ 1 km/s. Spectra containing lines of more than one star were analyzed with TODCOR—the two-dimensional correlation algorithm.

Results. The measured radial velocities confirmed the binarity of seventy of the BEER candidates—45 single-line binaries, 18 double-line binaries, and 7 diluted binaries. We show that red giants introduce a major source of false candidates, and demonstrate a way to improve BEER's performance in extracting higher-fidelity samples from future searches of CoRoT lightcurves. The periods of the confirmed binaries span a range of 0.3–10 days, and show a rise in the number of binaries per $\Delta \log P$ towards longer periods. The estimated mass ratios of the double-line binaries and the mass-ratios assigned to the single-line binaries, assuming an isotropic inclination distribution, span a range of 0.03–1. On the low-mass end we have detected two brown-dwarf candidates on a ~ 1 day period orbit.

Conclusions. This is the first time non-eclipsing beaming binaries are detected in CoRoT data, and we estimate that ~ 300 such binaries can be detected in the CoRoT long-run lightcurves.

Key words. binaries: spectroscopic - binaries: eclipsing - brown dwarfs - Techniques: photometric - Techniques: spectroscopic - Techniques: radial velocities

1. Introduction

The space-based photometric surveys CoRoT (Rouan et al. 1998; Baglin 2003) and *Kepler* (Borucki et al. 2010) were designed mainly to detect minute exoplanetary transits. Each of these missions has provided over 160,000 continuous stellar lightcurves with time-span of tens to hundreds days, and photometric precision of 10^{-3} – 10^{-4} per measurement (Auvergne et al. 2009; Koch et al. 2010). Hundreds of transiting planets were indeed detected (e.g., Moutou et al. 2013; Rowe et al. 2014), but the unprecedented-quality lightcurves enabled also the detection of other flux variations of astrophysical origins. One such variation is the relativistic beaming effect.

Rybicki & Lightman (1979) show that several factors contribute to the beaming effect, which increase (decrease) the observed brightness of any approaching (receding) light source by $\sim |4v_R/c|$, where v_R is the radial velocity (RV) of the source and c is the speed of light. Thus, for short-period (1–10 days) brown-dwarfs (BDs) or massive planetary companions ($M_p \sin i \gtrsim 5M_J$) of solar-like stars the beaming amplitudes are in the range of 10^{-4} – 10^{-5} . Loeb & Gaudi (2003) have predicted that *Kepler*'s

photometric precision would be sufficient to detect such companions. For stellar binaries with typical RV semi-amplitudes of $10 - 100 \text{ km s}^{-1}$, the beaming amplitudes are in the range of 10^{-3} – 10^{-4} . For this reason, Zucker, Mazeh, & Alexander (2007) have predicted that CoRoT and *Kepler* will detect also hundreds of non-eclipsing such binaries, and create a new observational category: beaming binaries.

Soon after the first *Kepler* lightcurves became available, several studies measured the beaming effect of a few eclipsing binaries (EBs) detected by *Kepler* (e.g., van Kerkwijk et al. 2010; Carter et al. 2011). However, as mentioned by Loeb & Gaudi (2003) and by Zucker, Mazeh, & Alexander (2007), for short-period binaries and planets, the beaming effect might be comparable to (or even smaller than) another two photometric effects—the ellipsoidal and the reflection light variations. The ellipsoidal variation is caused by tidal interactions between the two components of the binary (e.g., Morris 1985; Mazeh 2008). The reflection variation is caused by the brightness difference between the 'day' side and the 'night' side of each component (e.g., Wilson 1990; Harrison et al. 2003). Accounting for

the three effects, several studies succeeded to detect the small beaming effect caused by a transiting BD or even a transiting massive planet in CoRoT and *Kepler* lightcurves (e.g., Mazeh & Faigler 2010; Shporer et al. 2011; Mazeh et al. 2012; Jackson et al. 2012; Mislis et al. 2012).

To find *non-eclipsing* short-period beaming binaries, Faigler & Mazeh (2011) introduce the BEER algorithm, which searches lightcurves for a *combination* of the three photometric effects caused by a short-period companion—the BEaming, Ellipsoidal, and Reflection periodic modulations. BEER approximates each of the three effects by a sine/cosine function, relative to phase zero taken at the time of conjunction—when the lighter component is in front of the heavier one. The reflection and the beaming effects can then be approximated by cosine and sine functions with the orbital period, respectively, while the ellipsoidal effect can be approximated by a cosine function with half the orbital period.

Detection of BEER-like modulations in a stellar lightcurve does not yet prove the binary nature of the star, since sinusoidal flux modulations could be produced by other effects too (e.g., Aigrain et al. 2004). To confirm BEER detections one needs to perform RV follow-up observations (Faigler & Mazeh 2011). The first RV confirmation of non-eclipsing beaming binaries was reported by Faigler et al. (2012). Candidate binaries for that study were detected with BEER in Q0-Q2 *Kepler* lightcurves, and seven of them were confirmed using RV measurements.

Paper I of the current series (Faigler et al. 2013) reports the discovery of Kepler-76b—the first hot Jupiter discovered with BEER. In Paper II, Faigler & Mazeh (2015) show evidence for equatorial superrotation of three hot Jupiters measured by *Kepler*—KOI-13, HAT-P-7, and Kepler-76b.

In this paper we present RV confirmation of seventy new beaming binaries found by BEER in CoRoT lightcurves. The targets were selected from the first five long-run center CoRoT fields, and confirmed using the AAOMega multi-object spectrograph (Lewis et al. 2002). Section 2 presents the BEER search applied to the CoRoT lightcurves, Section 3 describes the spectroscopic follow-up observations, Section 4 details the spectral analysis and derivation of RVs from the spectra, Section 5 explains the orbital solutions performed and the statistical methods applied to separate true BEER binaries from false detections, Section 6 discusses the use of the findings to evaluate the BEER algorithm performance, Section 7 focus on the mass-ratio and orbital-period distributions of the new binaries, and Section 8 summarizes the findings.

2. The BEER photometric search for binaries

To detect beaming-binary candidates, we analyzed the $\sim 40,000$ white lightcurves of the CoRoT fields LRc01, LRc02, LRc03, LRc04, and LRc05. We did not use the red, green, or blue lightcurves of targets having chromatic information (e.g., Aigrain et al. 2008; Deleuil et al. 2011) due to their lower signal-to-noise ratio (SNR).

Lightcurve analysis consisted of several steps. First, over-sampled lightcurves (Surace et al. 2008) were rebinned back to 512 s. Then, we corrected for jumps in all lightcurves. Jumps were identified by calculating a median filter to each lightcurve and detecting outliers in its derivative. The correction was done by subtracting the median filter from the lightcurve around the identified jump epoch. A cosine transform based detrending and 4σ outliers removal were then performed using ROBUSTFIT (Holland & Welsch 1977). Next, an FFT-based power spectrum

(PS) was calculated for each lightcurve, and the five most prominent peaks were identified and analyzed following Faigler et al. (2013). As detailed there, for each of the five peaks we derived the BEER amplitudes and the estimated mass and albedo of the presumed companion by fitting the amplitudes with a BEER model, assuming that the orbit is circular and the peak corresponds to either the orbital period or half the orbital period. Hence, for each lightcurve we evaluated ten possible orbital periods.

After fitting a circular BEER model to each lightcurve at each of its suspected periods, we assigned each fit a score in the 0–1 range, with 1 being the best. The score of each fit was calculated as

$$S_{\text{Total}} = S_{\text{BEER_SNR}} S_{\text{min_SNR}} S_{\chi^2} S_{\sin i} S_{\text{Albedo}}, \quad (1)$$

where $S_{\text{BEER_SNR}}$ is the BEER model SNR score, $S_{\text{min_SNR}}$ is the score of the minimum SNR of the two BEER harmonics, S_{χ^2} is the fit χ^2 score, $S_{\sin i}$ is the score of the model-derived $\sin i$ and S_{albedo} is the score of the model-derived geometric albedo. Each of these partial scores is the result of a dedicated scoring function that gives a score in the range of 0–1 for its associated parameter. The scoring functions we used were

$$S_{\text{BEER_SNR}} = 1 - \exp\left(-\frac{\text{BEER_SNR}}{C_{\text{BEER_SNR}}}\right), \quad (2)$$

$$S_{\text{min_SNR}} = 1 - \exp\left(-\frac{\text{min_SNR}}{C_{\text{min_SNR}}}\right), \quad (3)$$

$$S_{\chi^2} = \exp\left(-\frac{\chi^2}{C_{\chi^2}}\right), \quad (4)$$

$$S_{\sin i} = 1 - \exp\left(-\frac{\sin i}{C_{\sin i}}\right), \quad (5)$$

$$S_{\text{Albedo}} = \exp\left(-\frac{\max(\text{Albedo} - C_{\text{alb_m}}, 0)}{C_{\text{alb_s}}}\right), \quad (6)$$

where $C_{\text{BEER_SNR}}$, $C_{\text{min_SNR}}$, C_{χ^2} , $C_{\sin i}$, $C_{\text{alb_m}}$, and $C_{\text{alb_s}}$ are constants that calibrate the behavior of the scoring functions. The most likely orbital period of each lightcurve was selected as the period with the highest total score S_{Total} , out of its ten evaluated periods.

As an illustration, Figures 1 and 2 show the lightcurve analysis of CoRoT 105962436 and CoRoT 104674562, respectively. Presented are 70-day long parts of the original and detrended lightcurves, the entire lightcurve power spectra, and the entire phase-folded and binned lightcurves, with the best-fit BEER models on top of them. Note that the most prominent peak in Figure 1 at 1.11 day^{-1} is caused by the ellipsoidal effect, whose frequency is double the orbital one (i.e. the predicted orbital period is 1.8 days). In Figure 2 it can be seen that the BEER modulation of CoRoT 104674562 at a period of 4.6 days is almost buried in the noise, and from the PS it seems that the modulation at ~ 20.4 days is more evident. Nevertheless, thanks to its period-selection process, BEER found the right orbital period in this case too (as we show in Section 5).

After the score assignment and the best period selection, we visually inspected the 200 highest-score candidates of each field and assigned priorities of 1–3 to targets that we deem viable binary candidates, with priority 1 assigned to the best candidates. These priorities were assigned through visual inspection of the photometric power spectrum, the goodness-of-fit of the BEER

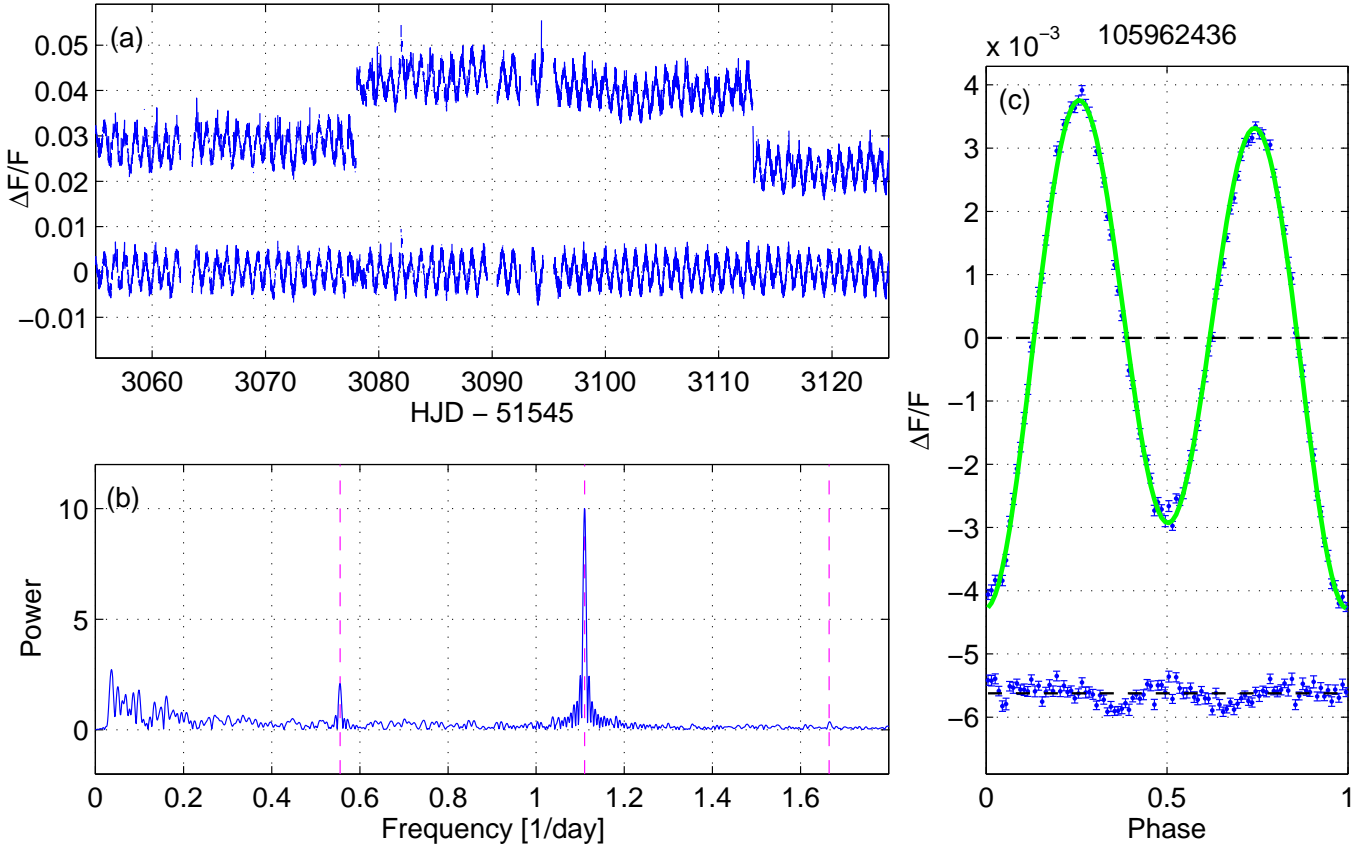


Fig. 1. BEER’s lightcurve analysis of CoRoT 105962436 (a) A 70-day long part of the CoRoT white lightcurve, normalized by its median. For clarity, the original lightcurve was shifted upwards by 0.03 relative to the cleaned and detrended one. The cleaned lightcurve demonstrates the jumps correction, outlier removal and detrending functionality. (b) FFT-based power spectrum of the detrended lightcurve, with its maximum value normalized to 10. Vertical dashed lines mark the first three harmonics of the candidate orbital frequency. (c) Phase-folded and binned lightcurve (blue) and the best-fit BEER models assuming a circular orbit (green). The residuals were shifted downwards for clarity.

model, the correlation structure of the time domain residuals and other target specific features. Naturally, the visual inspection method and the resulting target priorities are subjective and prone to human bias and errors, but we nevertheless use it for lack of a better software based method at this stage.

Consequently, we selected a total of 481 candidates for RV follow-up from all five fields. The assigned priorities of these candidates were later used by the AAOmega fiber-allocation software to prioritize between them in cases of conflicts. The selected candidates span a range of 0.1–17 days in predicted orbital period and of 0.3–87 mmag in photometric amplitudes. As we show later, the confirmed candidates span somewhat narrower ranges of 0.3–10 days in orbital period and of 0.5–87 mmag in photometric amplitudes.

3. AAOmega follow-up observations

We performed RV follow-up observations with the AAOmega multi-object spectrograph (e.g., Lewis et al. 2002; Smith et al. 2004; Saunders et al. 2004) at the Anglo-Australian Telescope (AAT). AAOmega’s 2-degree field of view, its 3-magnitude dynamic range, and its ability to record up to 392 spectra simultaneously are ideal for our purpose. These features enabled us to observe the majority of BEER candidates in each of the CoRoT fields in a single pointing. We used the AAOmega software

CONFIGURE (e.g., Lewis et al. 2002; Miszalski et al. 2006)¹ to optimize the pointing and fibre allocation. Table 1 lists for each field the selected pointing ephemeris, the number of BEER targets observed, and the total number of science targets observed. The observed stars span the range of 12.5–16 in V magnitude.

In total, we observed 281 out of the 481 selected BEER candidates. Most of the candidates that were selected for follow-up but not observed are from the LRc01 and LRc02 fields. These two fields were observed by CoRoT with *two* $1.4^\circ \times 1.4^\circ$ detectors, as opposed to the LRc03, LRc04, and LRc05 fields that were observed by CoRoT with only one such detector (Moutou et al. 2013). Nevertheless, to maximize the number of priority 1 candidates observed each night, we used only one pointing per field. Table 2 lists the coordinates, magnitudes, photometric ephemeris, and amplitudes of the three BEER effects for the candidates observed with AAOmega. For convenience, the confirmed binaries are indicated in the rightmost column of Table 2. In order to make the best use of available observing resources, we observed also several hundred CoRoT EBs. In this paper, however, we report only on observing *non-eclipsing* BEER candidates, and on confirming seventy of them. We leave the EBs spectra analysis to a separate paper.

¹ Available at <http://www.aao.gov.au/science/software/configure>.

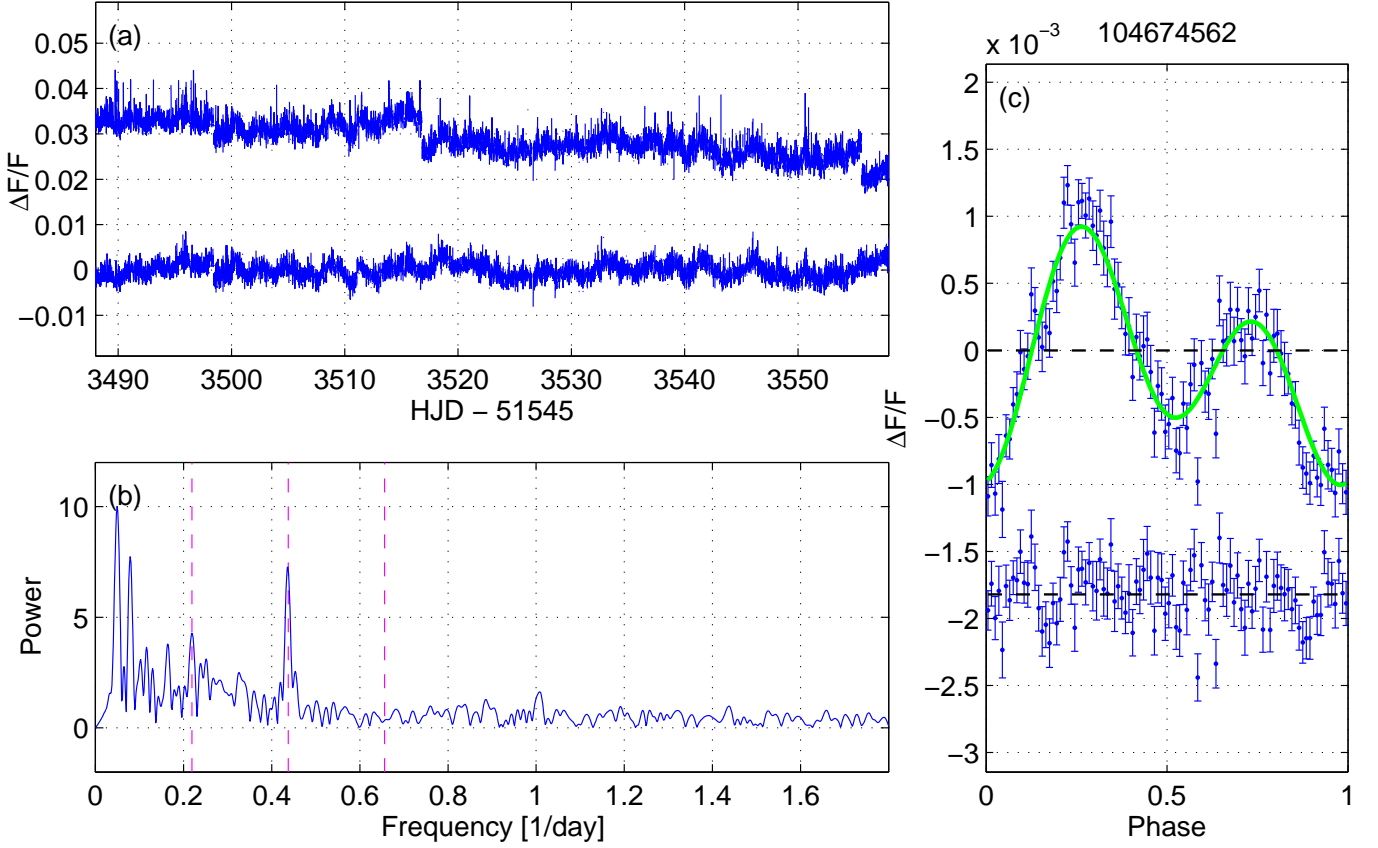


Fig. 2. BEER's lightcurve analysis of CoRoT 104674562. The panels are the same as in Figure 1.

Table 2. Coordinates and photometric parameters of the BEER candidates observed at AAOmega^a

CoRoT ID	RA (deg)	Dec (deg)	V (mag)	Orbital period (day)	Orbital phase (HJD-2451545)	Ellipsoidal amplitude (ppm)	Beaming amplitude (ppm)	Reflection amplitude (ppm)	conf. flag ^b
100537909	290.7709	1.2476	13.1	5.75 0.19	2828.9 2.5	-641 267	406 207	-216 204	1
100576007	290.8286	1.6783	15.1	0.319485 0.000074	2833.575 0.017	-902 27	227 21	-187 44	0
100604403	290.8710	1.6941	13.7	3.094 0.021	2832.39 0.50	-164 24	327 17	120 26	0
100637229	290.9165	1.4645	13.8	8.73 0.17	2829.7 1.4	-675 45	480 90	-148 88	0
100677124	290.9786	0.9625	15.7	0.41720 0.00015	2833.533 0.026	-9014 67	650 581	-1291 420	0

^(a) This table is available in its entirety in a machine-readable form in <ftp://wise-ftp.tau.ac.il/pub/corotAAO>. A portion of the table is shown here for guidance regarding its form and content. Note: each line of parameters is followed by a line of uncertainties.

^(b) conf. flag: 0—false alarm; 1—confirmed BEER binary.

Table 1. The selected pointing ephemeris of the five CoRoT fields, and the number of targets observed in each field.

Field	Mean RA (J2000)	Mean Dec (J2000)	Science targets	BEER targets
LRc01	19:26:25.34	+01:12:00.5	211	41
LRc02	18:41:52.44	+06:37:03.9	292	55
LRc03	18:32:27.45	-06:21:52.7	362	50
LRc04	18:33:50.89	+08:49:58.9	359	68
LRc05	18:39:19.29	+04:28:21.6	165	67

The observations took place on seven consecutive nights, starting on August 02, 2012. Between two and five fields were observed each night, depending on the available time and weather conditions. For most of the observed candidates we got six to seven AAOmega spectra. Table 3 lists for each field the heliocentric Julian dates (HJDs) of mid exposure, calculated for the mean ephemeris presented in Table 1.

On the red arm we used the 1700D grating since it was reported to give good RV precision (e.g., Lane et al. 2011). On the blue arm we used the 1700B grating since it covers several Balmer lines and enables RV measurements of hot stars too. The nominal spectral coverage is 8342–8842 Å on the red arm and

Table 3. Mid-exposure HJD–2456141 days.

LRc01	LRc02	LRc03	LRc04	LRc05
1.070956	---	0.998684	---	---
2.050900	1.942608	1.888283	1.996221	2.103633
3.045416	2.936347	2.882764	2.989653	3.098236
4.053797	3.942036	3.887762	3.995172	4.110621
5.104335	4.942736	4.889214	4.996094	5.049920
6.109585	5.946059	5.889688	6.001038	6.055340
---	6.950716	6.899660	7.009869	7.059933

3803–4489 Å on the blue arm, but the actual coverage is smaller by up to ~ 60 Å and is different for different fibers, depending on their position on the detector.

Observations and data reduction were performed similarly to previously reported works (see e.g., Sebastian et al. 2012). In short, the observing sequence at each new pointing usually consisted of a flat and two arc frames followed by 3 or 2 exposures of 20 or 30 minutes, respectively.

Data reduction utilized the dedicated software 2DFDR (Taylor et al. 1996)². The spectrum from each fiber and each sub-exposure was first normalized by its flat and wavelength calibrated using the arc frames, rebinning the data onto the same linear wavelength scale to facilitate combining the sub-exposures. The throughput of each fiber in each sub-exposure was calculated using sky emission lines. An average sky spectrum was subtracted from the data using dedicated sky fibres. Finally, the sub-exposures were combined to give a single calibrated 60-minute exposure, weighting each sub-exposure by its flux level and rejecting cosmic ray hits.

Most of the exposures were made under bright sky, so the sky subtraction procedure left some residuals of telluric emission lines in the spectra. In addition, a few pixels in each spectrum were affected by bad columns of the detector. We replaced the values of the telluric-line residuals and the bad pixels with a smoothed version of the same spectrum, which was calculated using a moving median filter, 21-pixel wide. Additional 6σ outliers were later replaced the same way.

4. Spectral analysis

4.1. Non-composite spectra analysis

To derive the most precise RVs we first searched for an optimal theoretical template spectrum for each candidate, by maximizing the cross-correlation values between the candidate’s observed spectra and a set of synthetic Phoenix spectra (Hauschildt et al. 1999), calculated on a grid of effective temperature (T_{eff}), surface gravity ($\log g$), and metallicity ($[M/H]$). Line broadening due to the projected rotational velocity was added to each synthetic spectrum by convolving it with a rotational profile $G(\nu)$ (e.g., Santerne et al. 2012; Gray 2005). To account for the instrumental broadening of the lines, each synthetic spectrum was also convolved with a Gaussian of $\sigma = 20.5 \text{ km s}^{-1}$.

Figures 3 and 4 illustrate the data and the optimization process. Figure 3 shows co-added AAOmega spectra and cross-correlation functions (CCFs) of four slowly rotating candidates (rotational broadening $\lesssim 20 \text{ km s}^{-1}$), which have different T_{eff} values and non-composite spectra. It can be seen how narrow metal lines weaken and wide Hydrogen lines become stronger as T_{eff} goes up. Accordingly, the CCF peaks of cool stars ($T_{\text{eff}} \lesssim 7000 \text{ K}$) are narrower than those of hot stars. Figure 4 shows

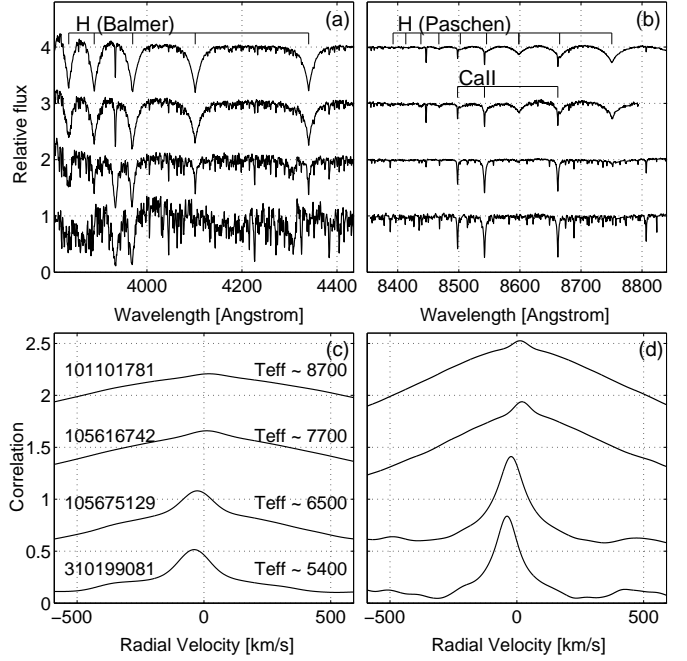


Fig. 3. Co-added AAOmega spectra (panels (a) and (b)) and CCFs (panels (c) and (d)) of four BEER candidates with different effective temperatures. For clarity, successive spectra were shifted upwards by 1 and successive CCFs were shifted upwards by 0.55. CoRoT IDs and estimated temperatures of the four candidates are indicated in panel (c). Blue-arm spectra and their CCFs are shown on the left (panels (a) and (c)), while red-arm spectra and their CCFs are shown on the right (panels (b) and (d)). Wavelengths of Ca II and Hydrogen lines are taken from Kramida et al. (2013).

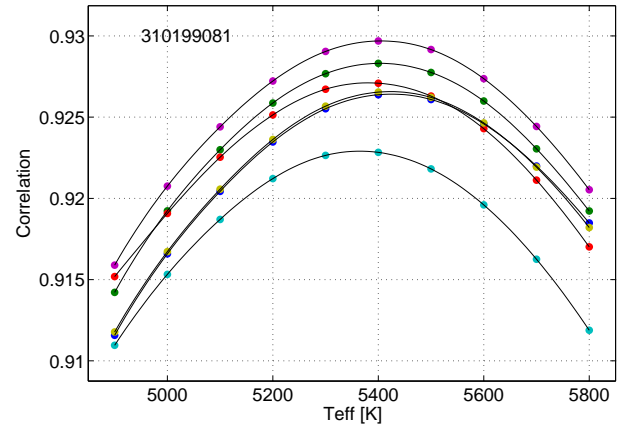


Fig. 4. T_{eff} optimization plot of CoRoT 310199081. Colored dots show the maximum-CCF values, cross-correlating its red-arm AAOmega spectra with synthetic Phoenix spectra of different T_{eff} . Solid-black lines show for each exposure a SPLINE interpolation of its maximum-CCF versus T_{eff} curve.

the T_{eff} optimization plot of the coolest candidate presented in Figure 3. The best T_{eff} for each exposure was estimated from the interpolation of its maximum-CCF versus T_{eff} curve. The best *global* T_{eff} for each candidate was taken as the weighted mean of the different T_{eff} values from the different exposures, taking the squares of the maximum-CCF values as weights. Surface grav-

² Available at <http://www.aao.gov.au/science/software/2dfdr>.

Table 4. Template parameters of non-composite spectrum candidates^a.

CoRoT ID	T_{eff} (K)	$\log g$ (cgs)	[m/H] (dex)	Rot. broad. (km s ⁻¹)	conf. flag
100537909	6500	5.0	0.0	7	1
100576007	5400	4.0	-0.5	1	0
100604403	7000	4.5	0.0	9	0
100637229	6500	4.5	0.0	16	0
100677124	6000	4.0	+0.5	102	0

^(a) This table is available in its entirety in a machine-readable form in <ftp://wise-ftp.tau.ac.il/pub/corotAAO>. A portion of the table is shown here for guidance regarding its form and content.

ity, metallicity, and projected rotational velocity were estimated for each candidate the same way. For each candidate, the nearest synthetic spectrum to its estimated spectral parameters was chosen as its best template.

The analysis, including RV derivation and orbital solutions, was performed both for the red-arm and blue-arm spectra, independently. However, the results presented from this point onwards are based on the red-arm spectra only, since we generally found them to have better SNR and stability than the blue-arm spectra. For instance, it can be seen in Figure 3 that the blue-arm CCF peaks are wider and lower than the red-arm CCF peaks of the same stars. This is partially due to the lower resolution and lower SNR of blue-arm spectra. Red-arm spectra thus provided better RV precision than blue-arm spectra, even for the hottest stars in the sample ($T_{\text{eff}} \gtrsim 8000$ K).

After optimizing the templates, we derived RVs and errors from each spectrum by calculating the CCF with the best template. At this stage we inspected carefully the CCFs, looking for a signature of a secondary star, and identified 26 stars that present composite spectra (i.e. spectra containing lines of more than one star). Table 4 lists the 255 non-composite spectrum candidates observed, and the template parameters used to derive their RVs. For convenience, the rightmost column identifies the confirmed BEER single-line binaries (SB1s), 45 of which were identified in that list (as explained in Section 5). The measured RVs of all non-composite spectrum candidates are given in a machine-readable form in <ftp://wise-ftp.tau.ac.il/pub/corotAAO>.

4.2. Composite spectra analysis

Composite spectra were analyzed with TODCOR (Zucker & Mazeh 1994; Mazeh & Zucker 1994)—the two-dimensional correlation algorithm. The optimization of the templates was done in several steps. First, we searched for the best primary template (i.e. the template for the more luminous component in the spectrum) similarly to the search performed for non-composite spectra. Inspecting the CCFs and the derived RVs we then identified for each candidate the exposures done at times when the separation between the primary and secondary sets of lines was relatively large. Using only these sub-sets of exposures we optimized the primary- and secondary-template T_{eff} and rotational broadening, optimizing also the flux ratio between the primary and the secondary components (TODCOR’s α parameter). Metallicity and $\log g$ of the secondary template (i.e. the template for the less luminous component in the spectrum) for each candidate were fixed assuming the secondary is a dwarf ($\log g = 4.5$) having the same metallicity as its primary.

After optimizing the templates, we used TODCOR to derive the primary and secondary RVs and errors from each spectrum, fixing α to its best value. As an illustration, Figure 5 shows a

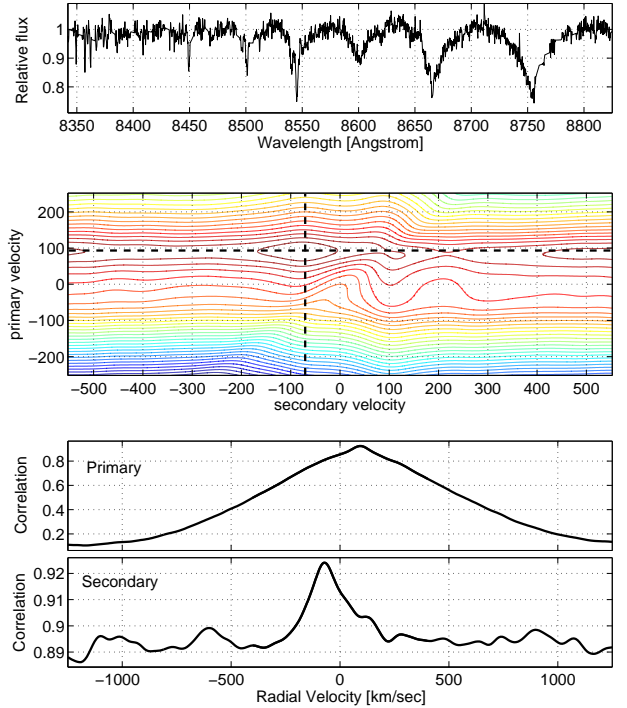


Fig. 5. Up: red-arm AAOmega spectrum of the double-line BEER binary 105962436 from August 05, 2012. Middle: TODCOR’s two-dimensional correlation function for that spectrum, using the templates whose parameters are specified in Table 5. Colored solid lines connect points of equal correlation. The black dashed lines run through the two-dimensional correlation peak parallel to the primary and secondary RV axes. Bottom: primary and secondary *cuts* through the two-dimensional correlation peak.

spectrum and the TODCOR plots for one of the AAOmega exposures of CoRoT 105962436—probably an A5V–G0V double-line binary (SB2) with $\alpha \sim 0.25$. The splitting of the Ca II lines can be seen in the upper panel. The middle panel shows the corresponding TODCOR’s two-dimensional correlation function. The lower panel of the figure shows the primary and secondary *cuts* (Zucker & Mazeh 1994) through the two-dimensional correlation function, which run through the two-dimensional correlation peak parallel to the primary and secondary RV axes. The correlation in the secondary cut drops only by ~ 0.03 when moving away from the peak, because we change the velocity of the *secondary* template, which contributes only $\sim 25\%$ of the light, and the primary velocity is kept at its best value. Nevertheless, the secondary peak is prominent, which means the RV of the secondary star *can* be measured despite the broad Hydrogen lines of the primary and the relatively low flux ratio.

Table 5 lists the template parameters and α values used for the composite-spectrum BEER candidates. We use the nomenclature ‘A’ and ‘B’ (both here and later in Table 8) only to denote the more and less luminous components, respectively. The measured RVs and errors of both components are given in a machine-readable form in <ftp://wise-ftp.tau.ac.il/pub/corotAAO>.

Table 5. Template parameters of the composite spectrum candidates^a.

CoRoT ID	T_{eff} (K)	$\log g$ (cgs)	[m/H] (dex)	Rot. broad. (km s ⁻¹)	Flux ratio (α)
100688131 A	6100	4.5	0.0	13	—
100688131 B	5900	4.5	0.0	6	0.62
100906796 A	7000	4.5	0.0	60	—
100906796 B	5100	4.5	0.0	71	0.15
100976101 A	7400	4.5	0.0	1	—
100976101 B	4800	4.5	0.0	16	0.09
101177998 A	7200	4.5	0.0	41	—
101177998 B	5000	4.5	0.0	14	0.17
103833966 A	6200	5.0	+0.5	1	—
103833966 B	5600	4.5	+0.5	21	0.27

^(a) This table is available in its entirety in a machine-readable form in <ftp://wise-ftp.tau.ac.il/pub/corotAAO>. A portion of the table is shown here for guidance regarding its form and content.

5. Orbital solutions

5.1. Confirming BEER binaries with non-composite spectra

To separate true BEER binaries from false detections (which we shall call for simplicity false alarms or FAs), and to derive the orbital parameters of the true BEER SB1s, we fitted the derived RVs of non-composite spectrum candidates with a circular Keplerian model. We calculated two χ^2 statistics— χ_{null}^2 and χ_{orb}^2 , for the null hypothesis (constant RV star) and for the circular orbital solution, respectively. We took the BEER period and phase as priors by treating them as additional *measurements*, meaning that their squares of residuals, scaled by their error estimates, were added to χ_{orb}^2 in the search for the best fit. For the best fit orbital parameters we calculated also the following F -statistic:

$$F = \frac{(\chi_{\text{null}}^2 - \chi_{\text{orb}}^2) / \text{DOF}_{\text{orb}}}{\text{DOF}_{\text{null}} - \text{DOF}_{\text{orb}}}, \quad (7)$$

where DOF_{null} and DOF_{orb} are the numbers of degrees of freedom of the null hypothesis and the orbital solution, respectively. Since the only free parameter of the null hypothesis is an RV offset, $\text{DOF}_{\text{null}} = N_{\text{RV}} - 1$, where N_{RV} is the number of RV points. For the orbital solution $\text{DOF}_{\text{orb}} = N_{\text{RV}} + 2 - p_{\text{orb}}$, where p_{orb} is the number of free-parameters of the orbital solution, since we treat the BEER period and phase as additional measurements. For a circular orbit $p_{\text{orb}} = 4$.

To get a good distinction between true BEER SB1s and FAs we used *both* the χ_{null}^2 -test and the F -test. The χ_{null}^2 -test was used first to screen all candidates that show no significant RV variability within the observing run. Then the F -test was applied to candidates that passed the χ_{null}^2 -test to check the compatibility of their RVs with a circular Keplerian model at the BEER-predicted period and phase. Only candidates that passed both tests were considered as confirmed BEER SB1s.

After visual inspection of the results, particularly of a few border-line cases, we have chosen the critical p -values to be 10^{-6} and 0.003 for the χ_{null}^2 - and F -tests, respectively. As a consequence, 54 out of the 255 non-composite spectrum candidates passed the χ_{null}^2 -test, and 45 of them passed also the F -test and were classified as confirmed BEER SB1s. The 9 candidates that passed the χ_{null}^2 -test but not the F -test might be true variables at a different orbital period, or their spectra suffer from some systematics causing RV outliers.

Another possible reason for a true BEER binary not to pass our F -test is an eccentric orbit. Therefore, we fitted each RV

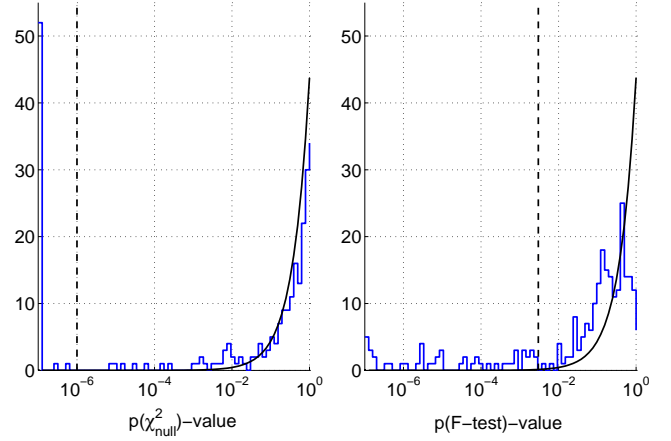


Fig. 6. Test statistics p -value histograms of the 255 non-composite spectrum BEER candidates, solving for their red-arm AAOmega RVs. The solid-black lines represent a flat distribution between 0 and 1 scaled so that its integral will be equal the number of FAs (210). The dashed-black lines mark the critical values that were chosen to separate possible BEER SB1s (to the left of the lines) from FAs (to the right of the lines). The histograms were truncated at 10^{-7} , so that the leftmost columns contain all candidates with p -values $< 10^{-7}$.

curve also with an eccentric Keplerian model, for which $p_{\text{orb}} = 6$. The fact we have only 6–7 RV points for most of our candidates makes DOF_{orb} of an eccentric solution to be as small as 2–3. Since F -test fails at such a low number of DOF, we required a p -value improvement of at least a factor of 10 to prefer the eccentric solution over the circular one. None of the candidates fulfilled this requirement, meaning we could not find significant eccentricity to any of the confirmed SB1s.

Figure 6 shows (on a log-scale) p -value histograms of the χ_{null}^2 - and F -statistics for the 255 non-composite spectrum BEER candidates. The solid-black lines represent the *expected* p -value distributions for RV measurements of constant-RV stars normally distributed for each star around its RV. There is a fair agreement between the expectation and the observed histograms, particularly for the χ_{null}^2 -statistics. The dashed-black lines mark the critical values that were chosen to separate possible BEER SB1s from FAs. Only candidates found to the left of the lines in *both* plots were considered as confirmed BEER SB1s.

Table 6 lists the orbital parameters of the confirmed BEER SB1s. Figure 12 shows their measured AAOmega RVs and the best-fit circular Keplerian model. Their orbital periods span a range of 0.4–10 days, and their RV semi-amplitudes span a range of 6–115 km s⁻¹. Two of the confirmed BEER SB1s with the smallest RV semi-amplitudes are CoRoT 105659320 and 101044188—possibly two BDs on a ~ 1 day period orbit around F-G stars.

5.2. Confirming BEER binaries with composite spectra

For a composite-spectrum candidate there are three possible scenarios. (1) The two components in the candidate’s spectra belong to the primary and secondary stars in a short-period SB2 at the BEER-predicted period and phase. (2) One of the components belongs to a binary at the BEER-predicted period and phase, while the other component belongs to another star, either bound or unbound to the binary (i.e. a *diluted* BEER binary). (3) Neither of the components belongs to the BEER-predicted

Table 6. Orbital parameters of the 45 confirmed BEER SB1s^a.

CoRoT ID	P (day)	T_0 (HJD-2456141)	K (km s ⁻¹)	γ (km s ⁻¹)	F -test p -value	χ_{orb}^2
103924393	6.851 0.021	5.906 0.021	49.93 0.75	42.90 0.60	1.3E-08	1.6
105767195	4.0526 0.0022	3.139 0.019	27.99 0.85	2.01 0.60	3.4E-08	0.7
105810223	0.5929447 0.0000029	3.87271 0.00097	115.0 1.4	4.31 0.93	4.0E-08	4.5
104674562	4.5804 0.0071	5.895 0.021	30.55 0.96	17.73 0.66	4.5E-08	0.7
310222016	2.08218 0.00047	5.725 0.020	29.3 1.7	-30.61 0.65	4.9E-08	3.8
310210722	6.975 0.020	7.165 0.025	47.7 1.2	11.02 0.78	1.1E-07	7.6
105818861	1.301182 0.000054	6.0599 0.0037	57.5 1.0	9.82 0.73	1.2E-07	3.5
101029997	3.57665 0.00044	3.361 0.011	41.42 0.88	36.17 0.59	1.3E-07	2.7
105844488	0.554937 0.000095	2.9081 0.0021	90.2 2.1	-7.7 1.5	1.4E-07	2.4
310215106	3.23943 0.00032	4.099 0.016	33.58 0.91	-0.07 0.69	1.7E-07	7.4
310176634	1.26221 0.00058	5.877 0.013	17.1 1.1	-26.82 0.81	3.5E-07	0.5
105336757	2.356960 0.000096	6.059 0.011	32.78 0.86	-7.64 0.64	3.8E-07	3.0
105712106	3.4521 0.0020	7.165 0.010	47.04 0.78	-2.58 0.59	7.7E-07	10.4
105403147	2.9136 0.0019	5.876 0.012	35.37 0.79	22.14 0.59	1.1E-06	7.0
105706604	2.26769 0.00017	6.978 0.012	32.4 1.2	-17.00 0.69	2.2E-06	4.8
105714214	3.1309 0.0051	1.950 0.012	36.57 0.82	-10.49 0.60	2.4E-06	10.0
104295292	2.8685 0.0043	2.751 0.015	26.09 0.86	7.83 0.60	2.8E-06	5.1
110567660	1.238837 0.000091	3.9782 0.0054	49.5 1.5	-8.1 1.0	2.9E-06	6.0
101177265	0.6419480 0.0000050	4.0489 0.0038	36.4 1.5	35.2 1.0	3.0E-06	3.4
101014035	0.4596816 0.0000015	4.0441 0.0021	55.3 1.7	1.9 1.2	4.1E-06	7.6
100889978	10.160 0.026	0.734 0.093	27.38 0.80	7.84 0.98	5.4E-06	9.4
105661774	2.22043 0.00013	2.094 0.023	31.3 2.3	26.2 1.4	6.2E-06	2.0
105618890	2.6219 0.0012	1.774 0.013	39.5 1.1	21.24 0.81	6.5E-06	11.0

^(a) Note: each line of parameters is followed by a line of uncertainties.

binary. We classified a composite-spectrum BEER candidate as confirmed if the RVs of at least one of its components are compatible with a Keplerian model at the BEER-predicted period and phase.

To assign each composite-spectrum candidate its right scenario, and (in case of a true BEER binary) to derive its orbital parameters, we fitted a circular Keplerian model to its primary and secondary RVs *separately*, calculating also the p -value of the F -test in Equation 7. Candidates in which both component's SB1-model got a p -value < 0.001 were considered as confirmed BEER SB2s. If the SB1 model of only one of the components got a p -value < 0.001 , the candidate was considered as a diluted BEER binary. If both component's SB1-model got a p -value > 0.001 we considered the candidate as a FA. Similarly to non-composite spectrum candidates, the selected critical p -

value of 0.001 originates in a visual inspection of the results, particularly of a few border-line cases.

In our sample of 26 composite-spectrum candidates we found 18 BEER SB2s, 7 diluted BEER binaries, and one FA (CoRoT 310186704). For the confirmed BEER SB2s we then fitted also a circular SB2 Keplerian model for the two sets of RVs together. Together with the 45 confirmed BEER SB1s we have thus confirmed 70 new non-eclipsing BEER binaries.

In addition to a circular model, we fitted each RV curve also with an eccentric Keplerian model. Requiring a factor 10 improvement in the F -test p -value, we found no SB2s that show measurable eccentricity. As for diluted binaries, we found two candidates (104626523 A and 103833966 A) to have slightly eccentric orbits. However, the small eccentricities (~ 0.3) found for this two cases might as well be spurious, or at least inflated

Table 6. Continued.

CoRoT ID	P (day)	T_0 (HJD-2456141)	K (km s ⁻¹)	γ (km s ⁻¹)	F -test p -value	χ^2_{orb}
105802223	1.414011	3.826	18.0	34.40	7.6E-06	2.0
	0.000040	0.014	1.2	0.85		
100880613	0.893171	1.9956	36.0	59.9	8.0E-06	8.3
	0.000018	0.0069	1.3	1.1		
105760939	1.53138	3.847	22.7	36.56	8.3E-06	2.6
	0.00042	0.012	1.4	0.89		
104113878	2.22939	3.085	15.70	-25.11	2.5E-05	6.5
	0.00024	0.024	0.97	0.59		
103782315	5.372	6.737	15.9	-46.68	3.1E-05	2.9
	0.012	0.070	1.3	0.90		
310169750	0.6321732	2.8879	40.5	-3.8	3.4E-05	8.0
	0.000065	0.0058	2.0	1.5		
103922738	7.901	7.92	6.2	12.64	5.3E-05	0.5
	0.037	0.19	1.4	0.87		
104648865	1.446104	5.045	32.6	-21.2	6.3E-05	0.8
	0.000097	0.041	5.9	4.3		
104536524	3.12477	2.108	10.8	60.34	6.7E-05	2.6
	0.00100	0.052	1.1	0.79		
101058035	0.7647344	6.1885	21.3	10.57	8.6E-05	9.1
	0.000057	0.0079	1.3	0.95		
105378453	3.2362	5.099	19.77	-14.99	1.5E-04	23.1
	0.0075	0.021	0.83	0.58		
105597526	0.920035	2.934	39.0	-55.7	2.0E-04	7.1
	0.000029	0.023	3.7	5.8		
104667709	0.6984611	3.0336	25.1	-34.8	3.5E-04	13.1
	0.000056	0.0071	1.9	1.1		
105154613	4.587	1.459	9.36	38.69	5.0E-04	8.6
	0.026	0.064	0.88	0.59		
100537909	4.8190	2.534	24.41	31.81	5.6E-04	67.6
	0.0094	0.023	0.83	0.56		
105659320	0.706141	4.986	6.91	-1.18	6.7E-04	4.7
	0.000026	0.018	0.94	0.72		
101044188	1.368287	4.969	8.19	39.32	7.1E-04	6.9
	0.000075	0.021	0.94	0.62		
104279119	10.161	7.63	14.8	12.5	7.3E-04	15.2
	0.051	0.24	1.5	1.7		
104598628	2.75207	4.264	19.1	96.2	1.3E-03	6.5
	0.00061	0.056	2.8	1.8		
105164611	3.50481	4.532	23.8	4.0	1.4E-03	9.0
	0.00066	0.056	2.9	1.8		
100851348	0.854818	4.027	13.5	19.0	1.7E-03	4.0
	0.000012	0.023	2.5	2.0		
105472536	0.4066543	6.8778	34.0	-36.8	2.1E-03	4.8
	0.000092	0.0050	6.4	2.4		

(e.g., Lucy & Sweeney 1971). The preference for an eccentric orbital solution might also be a result of systematic RV errors caused by the presence of the second component in the spectra.

Table 7 lists the orbital parameters of the confirmed BEER SB2s, sorted by ascending F -test p -value of the primary. Table 8 lists the orbital parameters of the variable components in the diluted BEER binaries, sorted by ascending F -test p -value.

Figure 13 shows the measured AAOmega RVs and the best-fit Keplerian models of the confirmed BEER SB2s listed in Table 7. Figure 14 shows the measured AAOmega RVs and the best-fit Keplerian models of the variable components in the confirmed BEER diluted binaries listed in Table 8.

Figure 15 shows the phase-folded and binned lightcurves of all 70 confirmed BEER binaries, together with the best-fit circular BEER model. For convenience, the order of the plots in Figure 15 is the same as in Figures 12–14.

6. Performance of the BEER search algorithm

We are now in a position to evaluate the performance of the BEER algorithm in detecting short period binaries in the lightcurves of CoRoT long runs. This is possible in view of the large sample of confirmations and FAs that are reported here.

6.1. BEER-model priority, $M_2 \sin i$, and period

We start by looking into the priority classes that we manually assigned to candidates during the visual inspection stage. The left-hand side of Table 9 lists the number of binary confirmations and FAs per priority class within our sample. Obviously, BEER did not perform that well with its priority 3 candidates. This is not very surprising, as they did not look as good candidates in the first place, and were included in the observational campaign only due to the availability of fibers on the AAOmega spectrograph. Therefore, we decided to ignore priority 3 candidates in

Table 7. Orbital parameters of the 18 confirmed BEER SB2s^a.

CoRoT ID	P (day)	T_0 (HJD-2456141)	K_1 (km s ⁻¹)	K_2 (km s ⁻¹)	γ (km s ⁻¹)	F -test p -value A	F -test p -value B	χ_{orb}^2
105962436	1.8020 0.0062	5.917 0.012	83.5 1.2	133.8 3.0	27.74 0.78	5.6E-09	8.0E-05	20.3
106024478	3.013 0.012	4.1436 0.0068	65.25 0.98	66.2 1.1	-22.33 0.57	2.0E-07	5.4E-08	9.9
105649738	3.604 0.010	2.7189 0.0064	87.6 1.1	87.7 1.2	-7.47 0.57	2.0E-07	2.2E-07	8.4
105928477	1.6509 0.0048	4.9285 0.0063	74.3 1.2	74.7 2.3	-2.18 0.80	2.3E-07	1.6E-06	3.1
100688131	6.984 0.098	2.518 0.023	38.12 0.77	43.20 0.95	-13.84 0.47	1.7E-06	2.3E-06	25.1
310198235	1.713 0.011	6.873 0.019	99.7 2.8	113.4 3.7	7.55 0.61	2.0E-06	6.3E-07	74.8
100976101	4.738 0.025	0.856 0.018	67.22 0.73	113.0 2.9	-9.00 0.55	2.3E-06	2.2E-05	68.7
104369937	6.093 0.061	5.699 0.020	56.37 0.81	72.8 1.7	-16.58 0.54	2.6E-06	2.2E-04	54.7
105963904	6.048 0.044	5.062 0.010	67.26 0.76	81.7 1.5	-36.46 0.53	2.8E-06	4.7E-05	99.9
104181232	4.138 0.027	4.025 0.012	58.15 0.87	83.2 3.5	-0.64 0.65	4.0E-06	1.9E-04	34.1
105506915	0.6542 0.0048	3.083 0.016	25.50 0.98	123.4 5.0	-72.51 0.96	2.0E-05	4.8E-05	22.8
310136399	6.146 0.098	2.826 0.027	73.2 1.9	76.0 1.7	-7.10 0.97	3.3E-05	2.0E-05	96.8
101177998	1.6103 0.0044	4.0305 0.0056	26.5 1.7	156.8 4.1	40.59 0.91	2.8E-04	2.4E-04	32.7
310212616	0.35918 0.00047	3.8372 0.0016	96.7 3.6	149.0 3.7	-12.0 2.0	3.4E-04	1.1E-05	105.1
103838038	6.238 0.061	4.758 0.016	42.98 0.88	44.0 1.0	-8.99 0.48	3.8E-04	4.4E-05	192.2
310173237	0.29882 0.00033	2.0277 0.0025	85.5 3.9	132.2 4.6	-38.6 2.1	4.7E-04	3.9E-04	177.7
104432741	0.43955 0.00053	4.0074 0.0018	86.5 2.7	166.1 4.1	9.7 2.0	6.0E-04	1.3E-05	29.8
105583867	0.8567 0.0037	2.049 0.017	54.4 2.7	141.5 7.0	10.2 2.0	6.1E-04	1.4E-04	47.2

^(a) Note: each line of parameters is followed by a line of uncertainties.**Table 8.** Orbital parameters of the variable component in the 7 confirmed diluted BEER binaries^a.

CoRoT ID	P (day)	T_0^b (HJD-2456141)	K (km s ⁻¹)	γ (km s ⁻¹)	F -test p -value	χ_{orb}^2
310205770 B	5.543 0.014	5.218 0.019	56.8 1.5	3.51 0.94	4.9E-07	12.6
310193013 B	0.2801751 0.0000021	5.8446 0.0013	193.3 3.9	-0.3 3.3	1.5E-05	32.0
104791410 B	1.04457 0.00051	6.757 0.021	108 18	0 18	2.0E-05	5.2
104626523 A	7.354 0.052	2.99 0.22	28.2 1.6	4.7 1.5	1.1E-03	0.1
105423352 B	4.712 0.018	3.668 0.040	56.5 2.5	-24.0 1.8	2.6E-04	10.8
100906796 B	0.8974124 0.0000046	5.0351 0.0043	180.0 4.8	-6.9 3.2	3.5E-04	39.7
103833966 A	10.80 0.11	7.75 0.92	72 47	1 22	4.0E-03	0.4

^(a) Note: each line of parameters is followed by a line of uncertainties.^(b) For the eccentric binaries 104626523 A and 103833966 A the third column shows periastron time. The eccentricity of 104626523 A is 0.33 ± 0.09 and its longitude of periastron is 242 ± 15 deg. The eccentricity of 103833966 A is 0.32 ± 0.16 and its longitude of periastron is 121 ± 40 deg.

our performance analysis, and concentrate only on priority 1 and priority 2 candidates.

Two other parameters that determine the success of the BEER detection are the secondary mass and the orbital period, as the BEER amplitudes depend mostly on these two param-

Table 9. Confirmations and FAs per priority class, applying different *filters* to the sample^a.

Filter:	All candidates		$M_2 \sin i > 0.25M_\odot$		$M_2 \sin i > 0.25M_\odot$ and spectral type earlier than G7 for $P > 1.4$ day	
Priority	Confirmations	FAs	Confirmations	FAs	Confirmations	FAs
1	30	26	30	18	30	17
2	35	108	35	71	34	54
3	5	77	5	70	4	35

^(a) See text for the justifications of the chosen filters.

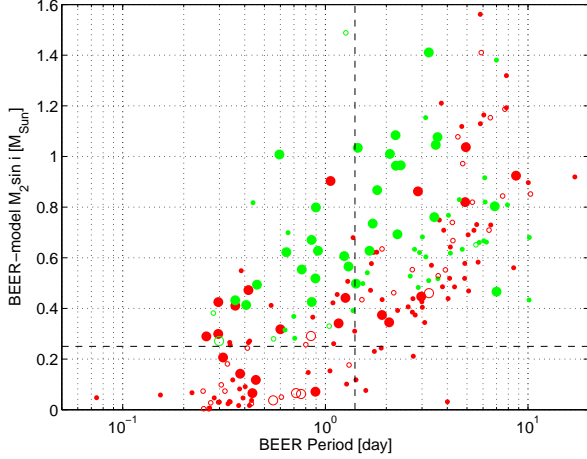


Fig. 7. The BEER-model $M_2 \sin i$ as a function of the BEER period. Large and small circles represent priority 1 and priority 2 targets, respectively. Green circles represent confirmations while red circles represent FAs. Open circles represent candidates of spectral type later than G7. The horizontal dashed line marks $M_2 \sin i = 0.25M_\odot$, below which there are no confirmed targets. The vertical dashed line marks $P = 1.4$ days, to the right of which there are 18 FAs of spectral type later than G7, but only one confirmed binary (See Section 6.2).

ters (Faigler & Mazeh 2011). We therefore plot in Figure 7 the BEER-model $M_2 \sin i$ as a function of the photometric period, for priority 1 and 2 targets. As expected, shorter-period modulations with larger BEER-model $M_2 \sin i$ have higher chances of being true BEER modulations rather than FAs. For instance, there are no confirmations with BEER-model $M_2 \sin i < 0.25M_\odot$. The vertical dashed line in Figure 7 marks $P = 1.4$ days, and it is explained next.

From this stage onward we continue the performance analysis while ignoring all targets with BEER-model $M_2 \sin i < 0.25M_\odot$. The summary of the remaining targets as a function of their priority is listed in the central columns of Table 9.

6.2. Spectral type

Another parameter that can influence the success of the BEER detection is the candidate’s spectral type. To check this option, we plot in Figure 8 the BEER score as a function of the spectral type for priority 1 and 2 candidates with BEER-model $M_2 \sin i > 0.25M_\odot$. The spectral type is taken from EXODAT³, and it was obtained using the SED analysis described by Deleuil et al. (2009). The advantage of using EXODAT is its availability regardless of any follow-up observations. It can be seen that there

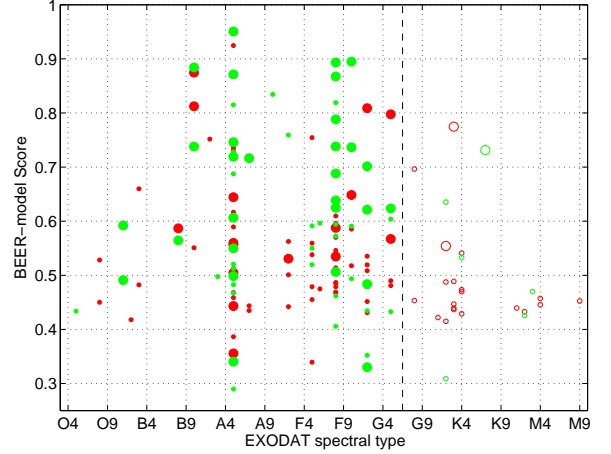


Fig. 8. BEER score as a function of the EXODAT spectral type for candidates with $M_2 \sin i > 0.25M_\odot$. The symbols are the same as in Figure 7. The vertical dashed line marks a spectral type of G7.

is a larger fraction of FAs for late-type candidates. Particularly, if we draw a line at a spectral type of G7 ($T_{\text{eff}} \sim 5600$ K), we find only 6 confirmed BEER binaries and 20 FAs to the right of that line.

In Figure 7 we also marked with open circles candidates of spectral type later than G7. A close examination of these cool candidates, with BEER-model $M_2 \sin i > 0.25M_\odot$, reveals that the confirmed binaries differ from the FAs in yet another way. Drawing a line at $P = 1.4$ days we find most of the cool FAs (18/20) to the right of that line, and most of the confirmed cool binaries (5/6) to the left of that line.

To explain this phenomenon, we plot in Figure 9 the spectral parameters of the observed candidates, which were derived in Section 4. Since spectral type is a proxy of T_{eff} , we place T_{eff} at the abscissa. Similarly to Figure 8, it can be seen that there is an excess of cool FAs ($T_{\text{eff}} \lesssim 5600$ K), with just a few confirmed binaries in that temperature regime. In addition, cool FAs seem to constitute a distinct sample of lower gravity, lower metallicity, slowly rotating stars. Despite the fact our spectral-parameter measurement technique is prone to systematic biases (e.g., Torres et al. 2012), we think that such a strong bimodality suggests that the majority of cool FAs are sub-giant or even red-giant stars.

We propose that the main reason red giants introduce false candidates with photometric periods of $\gtrsim 1.4$ day is related to solar-like oscillations. Using *Kepler* data Mosser et al. (2013) have shown that solar-like oscillations of $1\text{--}2M_\odot$ red giants have frequencies of $1\text{--}10\mu\text{Hz}$ (periods of 1.2–12 days), amplitudes (A_{max}) of 0.1–1 mmag, and that the amplitude *increases* with the period as a power law. For BEER binaries, the photometric am-

³ cesam.oamp.fr/exodat

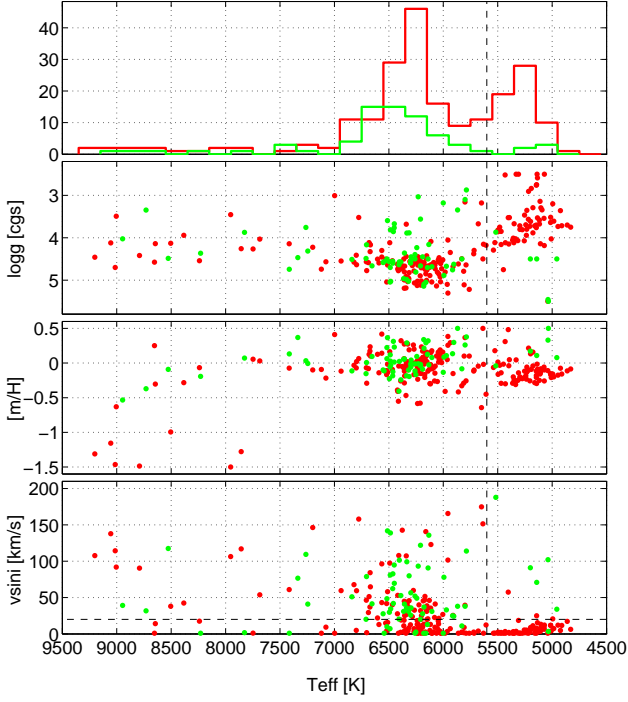


Fig. 9. The spectral parameters derived in Section 4. Confirmed BEER binaries represented in green, while FAs represented in red. For SB2s, only the spectral parameters of the primary are shown. For diluted BEER binaries, only the spectral parameters of the variable component are shown. Upper panel shows the two T_{eff} histograms. Lower three panels show the $T_{\text{eff}}\text{-log } g$, $T_{\text{eff}}\text{-metallicity}$, and $T_{\text{eff}}\text{-rotational broadening}$ scatter plots. Vertical dashed lines mark $T_{\text{eff}} = 5600\text{ K}$ —the approximate temperature of a G7V star. The horizontal dashed line in the lower panel marks rotational broadening of 20 km s^{-1} , below which the measured values are unreliable due to the medium resolution of the spectrograph (see Section 4).

plitude *decreases* with the period (Zucker, Mazeh, & Alexander 2007). However, it appears that for periods of about 1–10 days these two phenomena might have similar photometric amplitudes. A large fraction of the stars observed by CoRoT are indeed giants, particularly in the CoRoT-center fields (e.g., Deleuil et al. 2009; Gazzano et al. 2010). Despite the fact that solar-like oscillations are semi-regular in nature, given the typical length and SNR of long-run CoRoT data, BEER might have interpreted the variability of some red giants as an indication for the presence of a short-period companion.

To check whether filtering out red candidates with periods of > 1.4 days improves BEER’s performance, we list in the right-hand side of Table 9 the number of binary confirmations and FAs per priority class, after removing candidates with BEER-model $M_2 \sin i < 0.25M_{\odot}$, and also candidates of spectral type later than G7 having photometric periods of > 1.4 days. It can be seen that applying these two *filters* to the candidates list lowers the fraction of FAs to $\sim 1/3$ for priority 1 candidates, and to $\sim 2/3$ for priority 2 candidates.

6.3. BEER-model score

To evaluate the BEER performance as a function of its score, we count the targets with scores higher than some threshold T ,

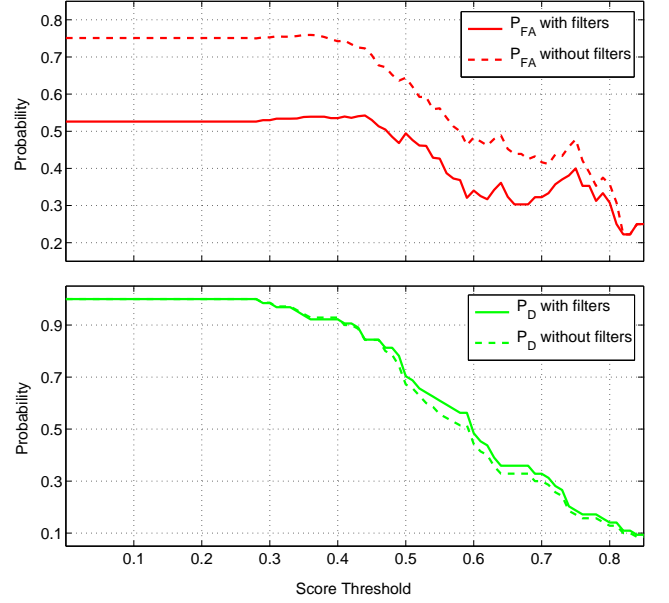


Fig. 10. Up: False-alarm probability as a function of the BEER score threshold. Down: The detection probability as a function of the BEER score threshold. Dashed lines show the probabilities for the whole sample of 281 candidates observed, while solid lines show the probabilities for the remaining 135 candidates, after applying the three filters discussed in the text (see also the first two rows of the right-hand side of Table 9). The plot was truncated at a score threshold of 0.85 since only 8 candidates got a higher score.

and obtain the detection probability $P_D(T)$ and the false-alarm probability $P_{FA}(T)$ of the algorithm as

$$P_D = \frac{\text{Number of confirmations with score} > T}{\text{Total number of confirmations}} \quad (8)$$

$$P_{FA} = \frac{\text{Number of false alarms with score} > T}{\text{Total number of targets with score} > T}. \quad (9)$$

To illustrate the algorithm performance, Figure 10 plots P_D and P_{FA} as a function of T for two sets of targets—the whole sample of 281 candidates observed, and the remaining 135 candidates, after filtering out priority 3 candidates, candidates with BEER-model $M_2 \sin i < 0.25M_{\odot}$, and candidates of spectral type later than G7 having photometric periods of > 1.4 day. It can be seen that the addition of these three filters lowers P_{FA} and raises P_D for any given T , hence improving the algorithm performance.

Estimating the two probabilities for any selected threshold level might be useful in estimating the results of future CoRoT-based BEER searches. Let us assume that, from the results of such a search, we select a sample of N targets with scores higher than some predefined threshold T . In such case, using the P_D and P_{FA} that correspond to T , we expect to have

$$N_C = N(1 - P_{FA}) \quad (10)$$

$$N_{FA} = NP_{FA} \quad (11)$$

$$N_{CC} = \frac{N(1 - P_{FA})}{P_D}, \quad (12)$$

where N_C is the number of expected confirmations within the N candidates, N_{FA} is the number of expected FAs within the N

Table 10. Spectral parameters, primary mass, and the assigned mass ratio of the 45 confirmed BEER SB1s.

CoRoT ID	T_{eff} (K)	$\log g$ (cgs)	[m/H] (dex)	Primary mass (M_{\odot})	Mass ratio (M_2/M_1)
103924393	6500	4.6	-0.1	1.20 ± 0.16	$0.69^{+0.70}_{-0.12}$
105767195	6400	4.6	-0.4	1.07 ± 0.13	$0.28^{+0.22}_{-0.04}$
105810223	6500	3.8	0.0	1.59 ± 0.38	$0.62^{+0.61}_{-0.11}$
104674562	6500	4.6	-0.2	1.15 ± 0.15	$0.32^{+0.16}_{-0.05}$
310222016	6800	4.5	-0.1	1.28 ± 0.17	$0.21^{+0.16}_{-0.03}$
310210722	7800	3.9	0.1	2.02 ± 0.46	$0.52^{+0.48}_{-0.09}$
105818861	6400	4.6	-0.2	1.12 ± 0.15	$0.41^{+0.36}_{-0.06}$
101029997	6600	4.6	-0.1	1.20 ± 0.15	$0.41^{+0.39}_{-0.06}$
105844488	5000	5.5	+0.3	1.01 ± 0.23	$0.53^{+0.50}_{-0.09}$
310215106	6300	3.9	-0.2	1.40 ± 0.32	$0.28^{+0.23}_{-0.05}$
310176634	5000	5.5	+0.5	1.07 ± 0.26	$0.10^{+0.20}_{-0.02}$
105336757	6500	4.6	-0.2	1.16 ± 0.15	$0.26^{+0.20}_{-0.04}$
105712106	6300	4.6	-0.0	1.15 ± 0.15	$0.48^{+0.43}_{-0.08}$
105403147	6700	4.5	-0.2	1.24 ± 0.17	$0.30^{+0.24}_{-0.02}$
105706604	6300	4.5	-0.1	1.15 ± 0.16	$0.26^{+0.20}_{-0.04}$
105714214	6200	5.1	0.2	1.19 ± 0.17	$0.33^{+0.27}_{-0.05}$
104295292	6200	4.7	-0.0	1.12 ± 0.14	$0.22^{+0.17}_{-0.02}$
110567660	6500	4.5	0.1	1.24 ± 0.17	$0.32^{+0.26}_{-0.05}$
101177265	6700	4.2	0.0	1.42 ± 0.27	$0.17^{+0.12}_{-0.03}$
101014035	6100	4.2	-0.0	1.24 ± 0.24	$0.25^{+0.19}_{-0.04}$
100889978	6300	5.0	-0.2	1.11 ± 0.14	$0.39^{+0.06}_{-0.15}$
105661774	8900	4.0	-0.5	1.96 ± 0.40	$0.20^{+0.15}_{-0.04}$
105618890	6300	4.4	0.0	1.20 ± 0.18	$0.34^{+0.28}_{-0.05}$
105802223	6400	4.6	0.0	1.20 ± 0.16	$0.11^{+0.08}_{-0.02}$
100880613	7300	4.5	+0.4	1.60 ± 0.22	$0.18^{+0.13}_{-0.03}$
105760939	6200	4.2	0.1	1.28 ± 0.23	$0.14^{+0.10}_{-0.02}$
104113878	6700	4.7	0.1	1.27 ± 0.15	$0.11^{+0.07}_{-0.02}$
103782315	5900	4.6	+0.3	1.12 ± 0.15	$0.16^{+0.11}_{-0.02}$
310169750	6500	3.6	+0.4	1.96 ± 0.52	$0.17^{+0.12}_{-0.03}$
103922738	6000	4.7	0.1	1.09 ± 0.14	$0.07^{+0.05}_{-0.01}$
104648865	8700	3.3	-0.4	2.89 ± 0.83	$0.15^{+0.06}_{-0.06}$
104536524	6400	4.4	0.1	1.25 ± 0.20	$0.08^{+0.06}_{-0.01}$
101058035	6500	4.7	0.1	1.23 ± 0.15	$0.11^{+0.07}_{-0.02}$
105378453	6300	5.0	-0.1	1.13 ± 0.14	$0.17^{+0.12}_{-0.02}$
105597526	6200	3.0	-0.0	2.47 ± 0.78	$0.17^{+0.13}_{-0.04}$
104667709	6200	3.6	-0.0	1.70 ± 0.46	$0.11^{+0.07}_{-0.02}$
105154613	6300	4.8	-0.2	1.08 ± 0.13	$0.09^{+0.06}_{-0.01}$
100537909	6500	5.0	-0.1	1.19 ± 0.15	$0.24^{+0.04}_{-0.01}$
105659320	6500	4.6	-0.1	1.16 ± 0.15	$0.03^{+0.02}_{-0.01}$
101044188	5900	4.8	0.1	1.07 ± 0.13	$0.05^{+0.03}_{-0.01}$
104279119	6200	5.1	+0.3	1.24 ± 0.18	$0.18^{+0.13}_{-0.02}$
104598628	6500	3.7	0.2	1.79 ± 0.46	$0.13^{+0.09}_{-0.03}$
105164611	8500	4.5	-0.1	1.75 ± 0.23	$0.18^{+0.13}_{-0.04}$
100851348	6300	3.9	+0.3	1.58 ± 0.36	$0.06^{+0.04}_{-0.01}$
105472536	5500	3.9	-0.0	1.20 ± 0.28	$0.14^{+0.10}_{-0.03}$

candidates, and N_{CC} is the estimated number of binaries that can be discovered by BEER in the original sample of CoRoT targets. For instance, using the solid lines in Figure 10, for $T = 0.6$ we get $P_{FA} \sim 1/3$ and $P_D \sim 1/2$. This means that, for $T = 0.6$, we expect about two thirds of the selected sample to be true BEER binaries, and the total number of BEER binaries in the original sample of CoRoT targets to be about $(4/3)N$.

7. The mass-ratio and orbital period distribution of the BEER CoRoT sample

To discuss the mass ratio and period distribution of the sample of confirmed BEER binaries, we wish to plot an estimate of the mass ratio of each system as a function of its orbital period. For SB2s this is straightforward, since the mass ratio

Table 11. Spectral parameters, primary mass, and mass ratio of the 18 confirmed BEER SB2s.

CoRoT ID	T_{eff} (K)	$\log g$ (cgs)	[m/H] (dex)	Primary mass (M_{\odot})	Mass ratio (M_2/M_1)
105962436	8200	4.4	-0.2	1.68 ± 0.26	0.62 ± 0.04
106024478	6000	3.2	-0.1	2.04 ± 0.63	0.99 ± 0.02
105649738	5800	3.1	+0.3	2.26 ± 0.71	1.00 ± 0.02
105928477	6300	4.4	-0.0	1.19 ± 0.18	0.99 ± 0.07
100688131	6100	4.7	0.1	1.14 ± 0.14	0.88 ± 0.02
310198235	6500	3.9	+0.3	1.66 ± 0.39	0.88 ± 0.12
100976101	7400	4.7	0.1	1.48 ± 0.16	0.60 ± 0.04
104369937	6400	5.0	0.1	1.18 ± 0.14	0.77 ± 0.03
105963904	6100	4.7	0.1	1.11 ± 0.14	0.82 ± 0.02
104181232	6500	5.0	-0.0	1.19 ± 0.15	0.70 ± 0.10
105506915	6500	3.8	0.0	1.62 ± 0.40	0.21 ± 0.04
310136399	5900	3.3	+0.5	2.04 ± 0.60	0.96 ± 0.06
101177998	7200	4.3	-0.0	1.50 ± 0.24	0.17 ± 0.03
310212616	6100	4.5	+0.3	1.22 ± 0.17	0.65 ± 0.11
103838038	6300	4.5	-0.1	1.13 ± 0.16	0.98 ± 0.03
310173237	5200	4.5	0.2	0.92 ± 0.14	0.65 ± 0.15
104432741	5800	2.9	+0.4	2.74 ± 0.90	0.52 ± 0.07
105583867	7300	3.8	0.0	1.92 ± 0.47	0.38 ± 0.14

$(q \equiv M_2/M_1 = K_1/K_2)$ can be measured directly from the orbital parameters. For SB1s, however, the mass ratio depends not only on the orbital parameters but also on the primary mass and orbital inclination, and can be found using the relation

$$(M_1 f^{-1} \sin^3 i) q^3 - q^2 - 2q - 1 = 0, \quad (13)$$

where M_1 is the estimated mass of the primary, f is the mass function derived analytically from the orbital parameters, and i is the inclination.

To estimate M_1 of the confirmed binaries we used the empiric relations given in Torres et al. (2010), which express a star's mass and radius in terms of its observed spectral parameters. As an input, we used the spectral parameters that were derived for the primary component of the confirmed SB1s and SB2s in Section 4. To estimate the mass uncertainties, we took equal uncertainties of 300 K in T_{eff} , 0.4 dex in $\log g$, and 0.3 dex in [m/H] to all primary stars. For most of the observed stars these uncertainties are larger than the scatter of the best spectral parameters between consecutive exposures (see for instance Figure 4), but taking into account the possible systematic errors (e.g., Torres et al. 2012), we think they are reasonable. The intrinsic scatter from the empiric relations (Torres et al. 2010) was added in quadratures to the mass uncertainties.

To assign an inclination for each SB1 we considered three options—to use the inclination estimated from its lightcurve by BEER, to derive its inclination distribution using the Mazeh & Goldberg (1992) algorithm, or to assume an isotropic inclination distribution. While using the BEER-model $\sin i$ estimates could sound appealing, we decided not to use them because we do not know their actual uncertainties, including possible systematic biases. Deriving inclination distributions using the Mazeh & Goldberg (1992) algorithm would probably be the right thing to do, but it is outside the scope of this paper. We therefore, somewhat arbitrarily, assigned a value of $\sin i = 0.866^{+0.121}_{-0.326}$, taking the median of an isotropic inclination distribution and the confidence limits to cover the central 68.3% of the distribution (e.g., Ho & Turner 2011; Lopez & Jenkins 2012).

Table 10 lists the spectral parameters, primary mass, and the assigned mass ratio of the confirmed BEER SB1s. Table 11 lists the primary spectral parameters, primary mass, and the estimated mass ratio of the confirmed BEER SB2s. For convenience, the

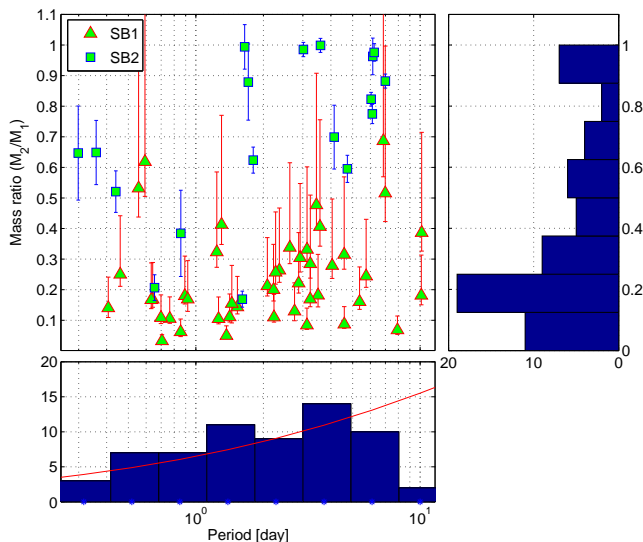


Fig. 11. Assigned mass ratio of the 45 confirmed SB1s and estimated mass-ratio of the 18 confirmed SB2s versus orbital period. For the SB1s we assumed an isotropic inclination distribution (see text). Bottom panel: period histogram. Solid-red line shows the Raghavan et al. (2010) log-normal fit to the period distribution of stellar binaries, scaled to best fit the histogram. Right panel: mass-ratio histogram.

order of Tables 10 and 11 is the same as of Tables 6 and 7, respectively. We did not estimate the masses of the seven diluted BEER binaries since their spectral parameters might have been biased by the presence of the third star.

Figure 11 shows the assigned mass ratio of the 45 confirmed SB1s, and the estimated mass ratio of the 18 confirmed SB2s, as function of their orbital period. The period and the mass-ratio histograms are plotted as well. The solid-red line in the period histogram shows the Raghavan et al. (2010) log-normal fit to the period distribution of stellar binaries in the solar neighborhood, scaled to best fit the histogram.

One feature that can be noticed in Figure 11 is that for periods of > 1 day, there seem to be a transition from SB1s to SB2s at $q \sim 0.6$. A similar transition was pointed out by Halbwachs et al. (2003) in their unbiased sample of solar-like spectroscopic binaries. In our sample this transition can be explained by the mass-luminosity relation of normal stars that is expected to be $L \sim M^4$ (e.g., Torres et al. 2010; Cox 2000, p. 382). Since the lowest significant α we could detect was ~ 0.1 (see Table 5), we did not expect detached binaries with $q \lesssim 0.6$ to be classified as SB2s. For periods of $\lesssim 1$ day this transition is less evident, since at such short periods some of these binaries could experience mass transfer via Roche-lobe overflow (e.g., Eggleton 1983), and the mass-luminosity relation deviates from that of isolated normal stars (e.g., Batten 1973, p. 154).

The period histogram clearly shows a rise in the number of binaries per $\Delta \log P$ from ~ 0.3 to ~ 6 days, followed by a sharp drop at periods of > 8 days. Since the detection probability of BEER binaries decrease with orbital period (see Figure 7), this rise is probably real. In the past three decades, several studies reported a log-normal period distribution of solar-like binaries, with a peak at $\log P \sim 5$ (e.g., Duquennoy & Mayor 1991; Raghavan et al. 2010), and it can be seen in Figure 11 that our period histogram fits well the Raghavan et al. (2010) log-normal fit out to $P \sim 8$ days. The scaling factor between the two sam-

ples is 1.61, which means that for bin size of $\Delta \log P = 0.214$, as we use here, we would get ~ 74 binaries at the peak of the distribution at $\log P = 5.03$. The histogram drops sharply at periods of > 8 days both because at such periods BEER approaches its sensitivity limit when applied to CoRoT long-run lightcurves, and because the AAOmega observing run was limited to seven nights.

The mass-ratio distribution of short-period binaries was the subject of several in-depth studies in the last three decades (e.g., Halbwachs 1987; Duquennoy & Mayor 1991; Mazeh et al. 1992; Halbwachs et al. 2003; Goldberg et al. 2003; Fisher et al. 2005). The main debates regarding the mass-ratio distribution of spectroscopic binaries are about the existence of peaks at $q \sim 1$ and/or at $q \sim 0.2$, and about the shape of the distribution towards lower q values—whether it is monotonically increasing, decreasing, or flat. It is therefore of interest to plot the distribution of the assigned mass ratios of our sample, as was done in Fig. 11.

The histogram presents three features, when going from top to bottom. (1) A clear peak at $q \sim 1$. (2) The number of binaries increases with decreasing q . (3) The histogram peaks at $q \sim 0.2$, and then falls sharply towards $q \sim 0.1$. However, correcting our sample for the Öpik (1924) effect might have diminished the $q \sim 1$ peak significantly (e.g., Goldberg et al. 2003; Halbwachs et al. 2003). In addition, at $q < 0.6$ our histogram is dominated by SB1s, and Mazeh & Goldberg (1992) have already shown that using an average $\sin i$ value to all SB1s, like we did here, might produce a monotonically increasing q distribution when the actual true distribution is flat. Lastly, the drop towards $q \sim 0.1$ can be explained both by BEER’s sensitivity for CoRoT long-run lightcurves, which probably approaches its limit at such low mass-ratios, and by the limited RV precision of our AAOmega data. Therefore, before reaching any definite conclusion, our data need in-depth analysis to derive a real mass-ratio distribution of the CoRoT BEER sample (Shahaf et al., in prep.).

8. Summary

We have presented AAOmega RV confirmation of seventy new non-eclipsing short-period binaries found by BEER in CoRoT lightcurves. The confirmed binaries span a range of 0.3–10 days in orbital period, showing a clear rise in the number of binaries per $\Delta \log P$ towards longer periods. Our spectral analysis shows that the primary stars in the detected binaries are typically of spectral type G or earlier, and the mass ratio (including the mass ratio assigned to SB1s) spans a range of 0.03–1. The mass-ratio histogram resembles a double-peak distribution (e.g., Halbwachs et al. 2003), but since we did not correct our results, neither for some well-known selection effects (e.g., Öpik 1924) nor for the non-isotropic inclination distribution (e.g., Mazeh & Goldberg 1992), the underlying true distribution might as well be flat. Nevertheless, the orbital solutions presented here can be used in the future for an in-depth study of the mass-ratio distribution of short-period binaries, similar to the study presented by Goldberg, Mazeh, & Latham (2003).

On the lower end of our detection capability, we have detected two BD candidates on a ~ 1 day period orbit around F-G stars. We consider them as BD *candidates* and not bona-fide BDs for two reasons—(1) the true inclination is not known, and (2) higher resolution and/or SNR spectroscopic observations might reveal in the future a faint companion, which could not have been found in the AAOmega spectra.

Relativistic beaming was already detected in CoRoT lightcurves (e.g., Mazeh & Faigler 2010), but this is the first time

that BEER detects *non-eclipsing* binaries in CoRoT lightcurves. To roughly estimate the expected number of such binaries that can potentially be detected with BEER in CoRoT long-run lightcurves we should correct first for the 200 binaries that were selected for follow-up but not observed, taking into account their BEER priorities, and then for the total number of CoRoT long-run lightcurves ($\sim 110,000$), assuming that short-period binaries do not have preference for center or anti-center fields. Doing so, we estimate that observing all 481 selected candidates would have brought the number of confirmed binaries to ~ 110 , and that the expected number of beaming binaries that can be detected in CoRoT long-run lightcurves is ~ 300 . This confirms the prediction made by Zucker, Mazeh, & Alexander (2007)—that CoRoT and *Kepler* will be capable of detecting hundreds of non-eclipsing beaming binaries.

Investigating BEER's false-alarm probability and nature in CoRoT long-run lightcurves, we have shown that red giants introduce a major source of false candidates, and demonstrated a way to improve BEER's performance in extracting higher-fidelity samples from future searches. Understanding the dependence of the fidelity and completeness of such future samples on parameters like period, spectral type, and BEER-model score, might enable using these samples to derive some statistical properties of the short-period binary population, like the period distribution, even before RV follow-up is done. Merging well-corrected large samples of CoRoT and *Kepler* beaming binaries with equivalent EB samples (e.g., Prša et al. 2011) might create large and well-defined samples of short-period binaries, which may shed some light on binary formation and evolution.

Radial-velocity follow-up observations of beaming and eclipsing binaries will continue to play a key role in these efforts, as in most cases this is the only way to measure their mass ratio and the mass of the secondary companion. Scaling the AAOmega time that was required to make the detections reported here, we estimate that only three additional such runs would be required to detect virtually all beaming binaries that can be detected in CoRoT long-run lightcurves. This demonstrates again the efficiency of using multi-object spectrographs for this task (e.g., Zucker, Mazeh, & Alexander 2007). One advantage of the beaming binaries over the EBs is the ability to detect binaries not only at edge-on inclinations, which widens the window for detecting intrinsically rare systems, like BD and massive-planetary companions to main-sequence stars (e.g., Halbwachs et al. 2000; Faigler et al. 2013).

Acknowledgements. We thank Gary Da Costa and Simon O'Toole for their help with preparing the AAOmega proposal and observations. We are grateful for the invaluable assistance of the AAOmega technical staff and support astronomers. Particularly, we thank Sarah Brough for her help with preparing, performing, and reducing the observations. We thank Gil Sokol for his help with the observations and the spectral analysis. We also thank the anonymous referee and the editor for their fruitful comments and suggestions. The research leading to these results has received funding from the European Community's Seventh Framework Programme (FP7/2007-2013) under grant-agreement numbers 291352 (ERC) and RG226604 (OPTICON). This research was also supported by the Israel Science Foundation (grant No. 1423/11), and by the Israeli Centers of Research Excellence (I-CORE, grant No. 1829/12). The CoRoT space mission, launched on 2006 December 27, was developed and operated by the CNES, with participation of the Science Programs of ESA, ESA's RSSD, Austria, Belgium, Brazil, Germany, and Spain.

References

Aigrain, S., Barge, P., Deleuil, M., et al. 2008, in *Astronomical Society of the Pacific Conference Series*, Vol. 384, 14th Cambridge Workshop on Cool Stars, Stellar Systems, and the Sun, 270–280

Aigrain, S., Favata, F., & Gilmore, G. 2004, *A&A*, 414, 1139

Auvergne, M., Bodin, P., Boissard, L., et al. 2009, *A&A*, 506, 411

Baglin, A. 2003, *Advances in Space Research*, 31, 345

Batten, A. H. 1973, *Binary and multiple systems of stars*

Borucki, W. J., Koch, D., Basri, G., et al. 2010, *Science*, 327, 977

Carter, J. A., Rappaport, S., & Fabrycky, D. 2011, *ApJ*, 728, 139

Cox, A. N. 2000, *Allen's astrophysical quantities*

Deleuil, M., Meunier, J. C., Moutou, C., et al. 2009, *AJ*, 138, 649

Deleuil, M., Moutou, C., & Bordé, P. 2011, *Detection and Dynamics of Transiting Exoplanets*, St. Michel l'Observatoire, France, Edited by F. Bouchy; R. Díaz; C. Moutou; EPJ Web of Conferences, Volume 11, id.01001, 110, 1001

Duquennoy, A. & Mayor, M. 1991, *A&A*, 248, 485

Eggleton, P. P. 1983, *ApJ*, 268, 368

Faigler, S. & Mazeh, T. 2011, *MNRAS*, 415, 3921

Faigler, S. & Mazeh, T. 2015, *ApJ*, 800, 73

Faigler, S., Mazeh, T., Quinn, S. N., Latham, D. W., & Tal-Or, L. 2012, *ApJ*, 746, 185

Faigler, S., Tal-Or, L., Mazeh, T., Latham, D. W., & Buchhave, L. A. 2013, *ApJ*, 771, 26

Fisher, J., Schröder, K.-P., & Smith, R. C. 2005, *MNRAS*, 361, 495

Gazzano, J.-C., de Laverny, P., Deleuil, M., et al. 2010, *A&A*, 523, A91

Goldberg, D., Mazeh, T., & Latham, D. W. 2003, *ApJ*, 591, 397

Gray, D. F. 2005, *The Observation and Analysis of Stellar Photospheres*, 3rd Edition, 465

Halbwachs, J. L. 1987, *A&A*, 183, 234

Halbwachs, J. L., Arenou, F., Mayor, M., Udry, S., & Queloz, D. 2000, *A&A*, 355, 581

Halbwachs, J. L., Mayor, M., Udry, S., & Arenou, F. 2003, *A&A*, 397, 159

Harrison, T. E., Howell, S. B., Huber, M. E., et al. 2003, *AJ*, 125, 2609

Hauschildt, P. H., Allard, F., & Baron, E. 1999, *ApJ*, 512, 377

Ho, S. & Turner, E. L. 2011, *ApJ*, 739, 26

Holland, P. W. & Welsch, R. E. 1977, *Commun. Statist. – Theor. Meth.*, 6, 813

Jackson, B. K., Lewis, N. K., Barnes, J. W., et al. 2012, *ApJ*, 751, 112

Koch, D. G., Borucki, W. J., Basri, G., et al. 2010, *ApJ*, 713, L79

Kramida, A., Yu. Ralchenko, Reader, J., & and NIST ASD Team. 2013, *NIST Atomic Spectra Database (ver. 5.1)*. [Online]. Available: <http://physics.nist.gov/asd> [2014, August 11]. National Institute of Standards and Technology, Gaithersburg, MD.

Lane, R. R., Kiss, L. L., Lewis, G. F., et al. 2011, *A&A*, 530, A31

Lewis, I. J., Cannon, R. D., Taylor, K., et al. 2002, *MNRAS*, 333, 279

Loeb, A. & Gaudi, B. S. 2003, *ApJ*, 588, L117

Lopez, S. & Jenkins, J. S. 2012, *ApJ*, 756, 177

Lucy, L. B. & Sweeney, M. A. 1971, *AJ*, 76, 544

Mazeh, T. 2008, *ArXiv e-prints*, 801

Mazeh, T. & Faigler, S. 2010, *A&A*, 521, L59+

Mazeh, T. & Goldberg, D. 1992, *ApJ*, 394, 592

Mazeh, T., Goldberg, D., Duquennoy, A., & Mayor, M. 1992, *ApJ*, 401, 265

Mazeh, T., Nachmani, G., Sokol, G., Faigler, S., & Zucker, S. 2012, *A&A*, 541, A56

Mazeh, T. & Zucker, S. 1994, *Ap&SS*, 212, 349

Mislis, D., Heller, R., Schmitt, J. H. M. M., & Hodgkin, S. 2012, *A&A*, 538, A4

Miszalski, B., Shortridge, K., Saunders, W., Parker, Q. A., & Croom, S. M. 2006, *MNRAS*, 371, 1537

Morris, S. L. 1985, *ApJ*, 295, 143

Mosser, B., Dziembowski, W. A., Belkacem, K., et al. 2013, *A&A*, 559, A137

Moutou, C., Deleuil, M., Guillot, T., et al. 2013, *Icarus*, 226, 1625

Öpik, E. 1924, *Publications of the Tartu Astrofizika Observatory*, 25, No 6

Prša, A., Batalha, N., Slawson, R. W., et al. 2011, *AJ*, 141, 83

Raghavan, D., McAlister, H. A., Henry, T. J., et al. 2010, *ApJS*, 190, 1

Rouan, D., Baglin, A., Copet, E., et al. 1998, *Earth Moon and Planets*, 81, 79

Rowe, J. F., Bryson, S. T., Marcy, G. W., et al. 2014, *ApJ*, 784, 45

Rybicki, G. B. & Lightman, A. P. 1979, *Radiative processes in astrophysics*

Santerne, A., Moutou, C., Barros, S. C. C., et al. 2012, *A&A*, 544, L12

Saunders, W., Bridges, T., Gillingham, P., et al. 2004, in *SPIE Conference Series*, ed. A. F. M. Moorwood & M. Iye, Vol. 5492, 389–400

Sebastian, D., Guenther, E. W., Schaffenroth, V., et al. 2012, *A&A*, 541, A34

Shporer, A., Jenkins, J. M., Rowe, J. F., et al. 2011, *AJ*, 142, 195

Smith, G. A., Saunders, W., Bridges, T., et al. 2004, in *SPIE Conference Series*, ed. A. F. M. Moorwood & M. Iye, Vol. 5492, 410–420

Surace, C., Alonso, R., Barge, P., et al. 2008, in *SPIE Conference Series*, Vol. 7019

Taylor, K., Bailey, J., Wilkins, T., Shortridge, K., & Glazebrook, K. 1996, in *Astronomical Society of the Pacific Conference Series*, Vol. 101, *Astronomical Data Analysis Software and Systems V*, ed. G. H. Jacoby & J. Barnes, 195

Torres, G., Andersen, J., & Giménez, A. 2010, *A&A Rev.*, 18, 67

Torres, G., Fischer, D. A., Sozzetti, A., et al. 2012, *ApJ*, 757, 161

van Kerkwijk, M. H., Rappaport, S. A., Breton, R. P., et al. 2010, *ApJ*, 715, 51

Wilson, R. E. 1990, *ApJ*, 356, 613

Zucker, S. & Mazeh, T. 1994, *ApJ*, 420, 806

Zucker, S., Mazeh, T., & Alexander, T. 2007, *ApJ*, 670, 1326

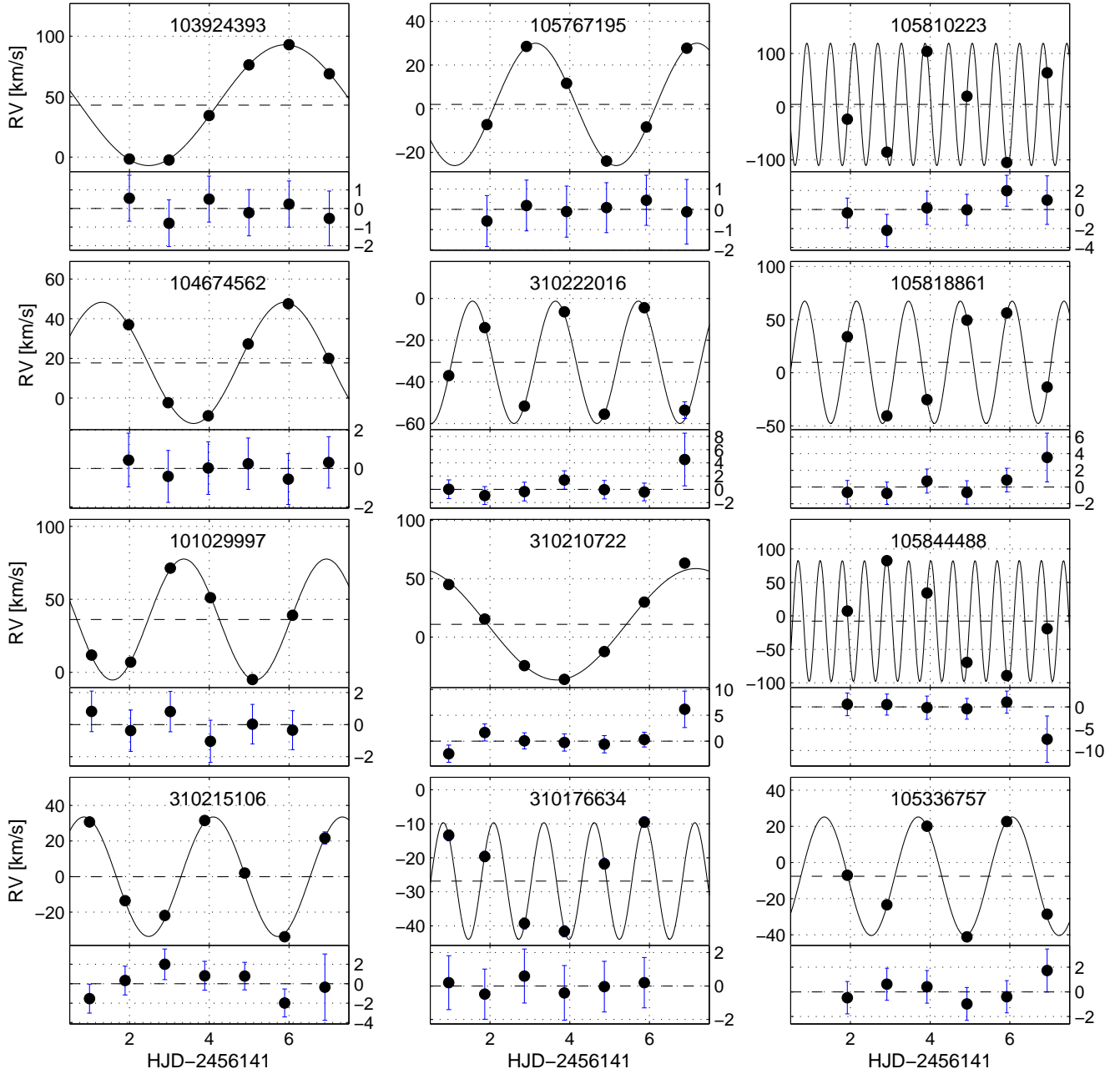


Fig. 12. AAOmega RVs (black circles) and the best-fit Keplerian models (solid lines) of the confirmed BEER SB1s listed in Table 6.

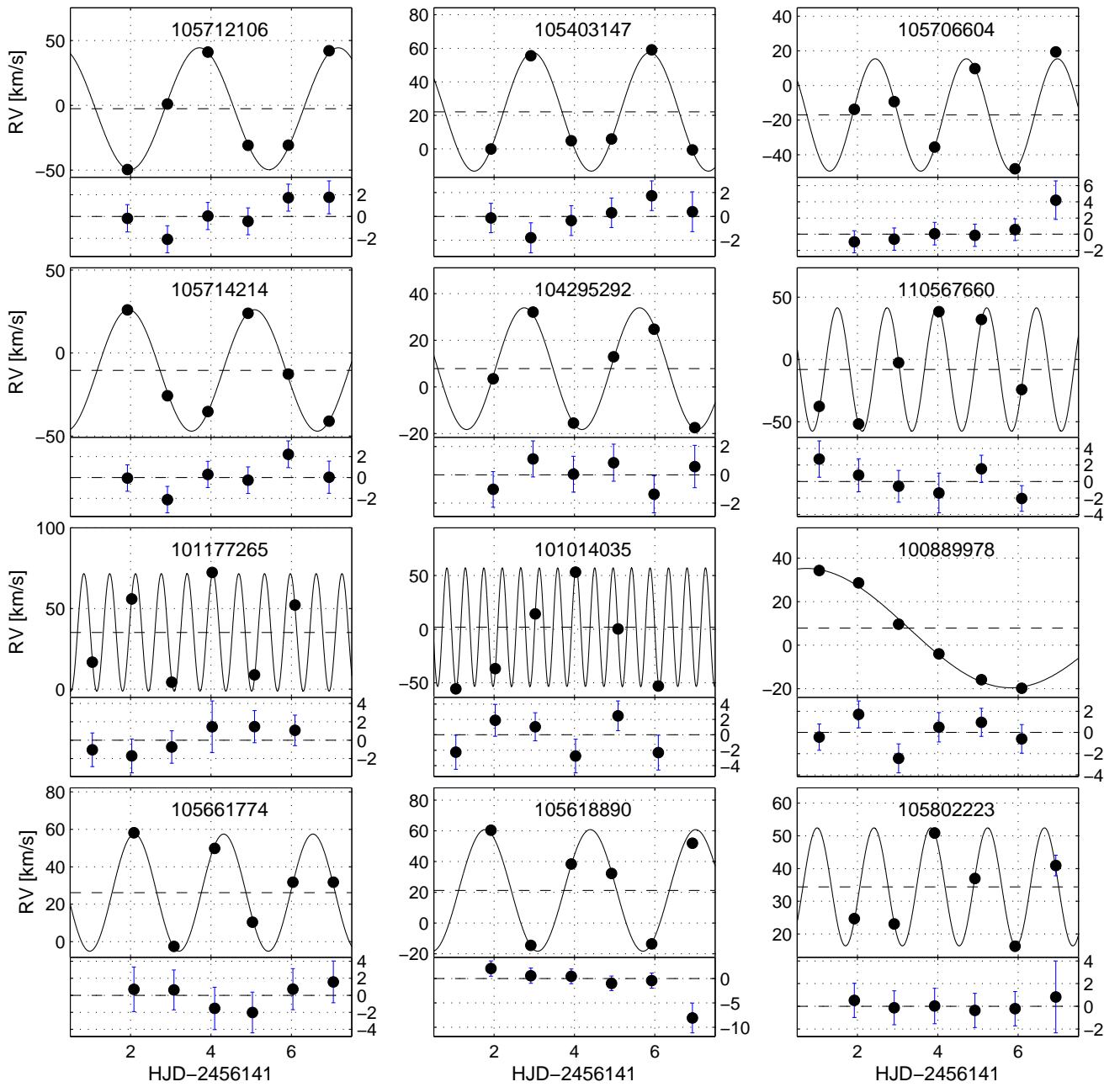


Fig. 12. Continued.

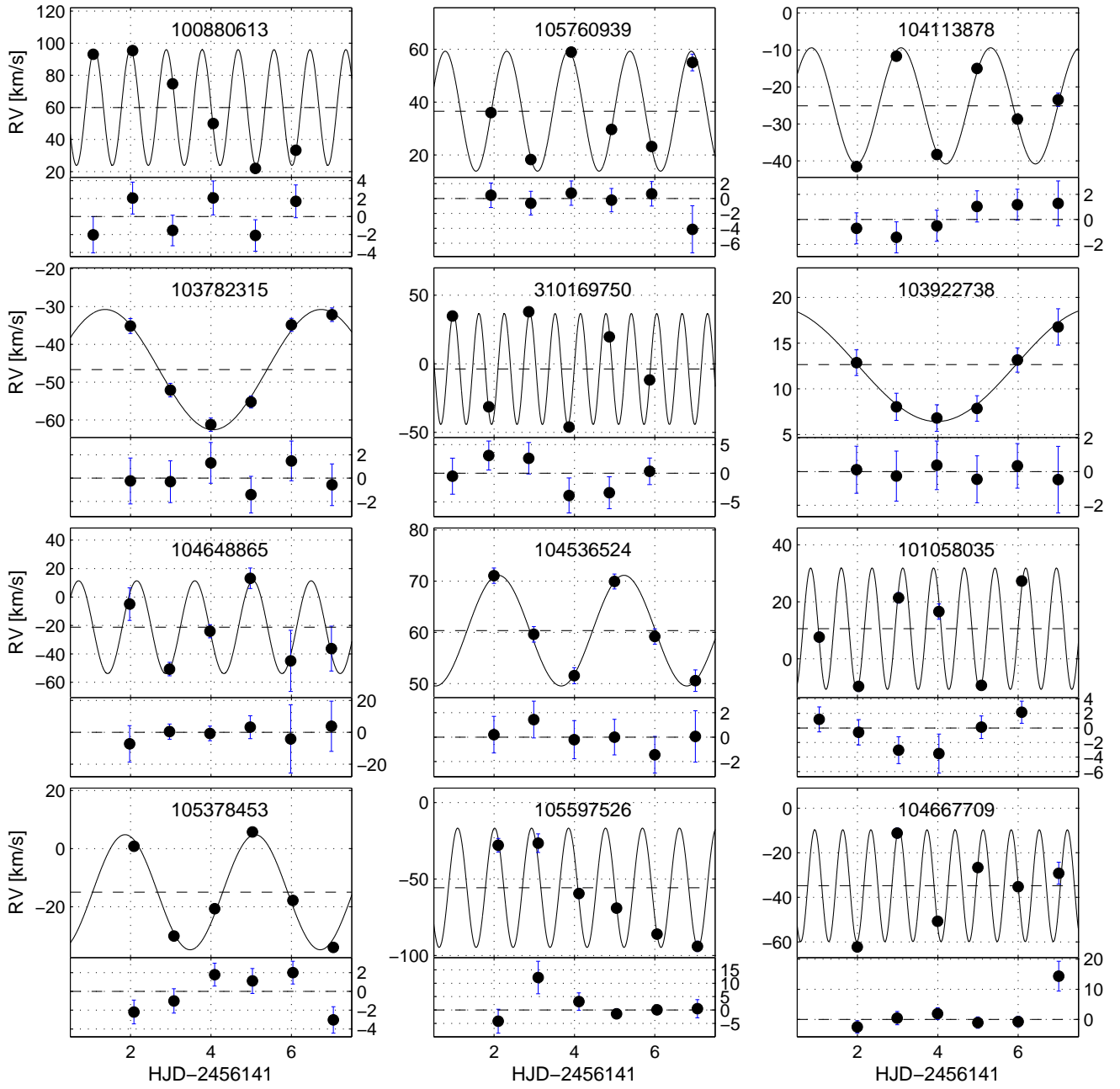


Fig. 12. Continued.

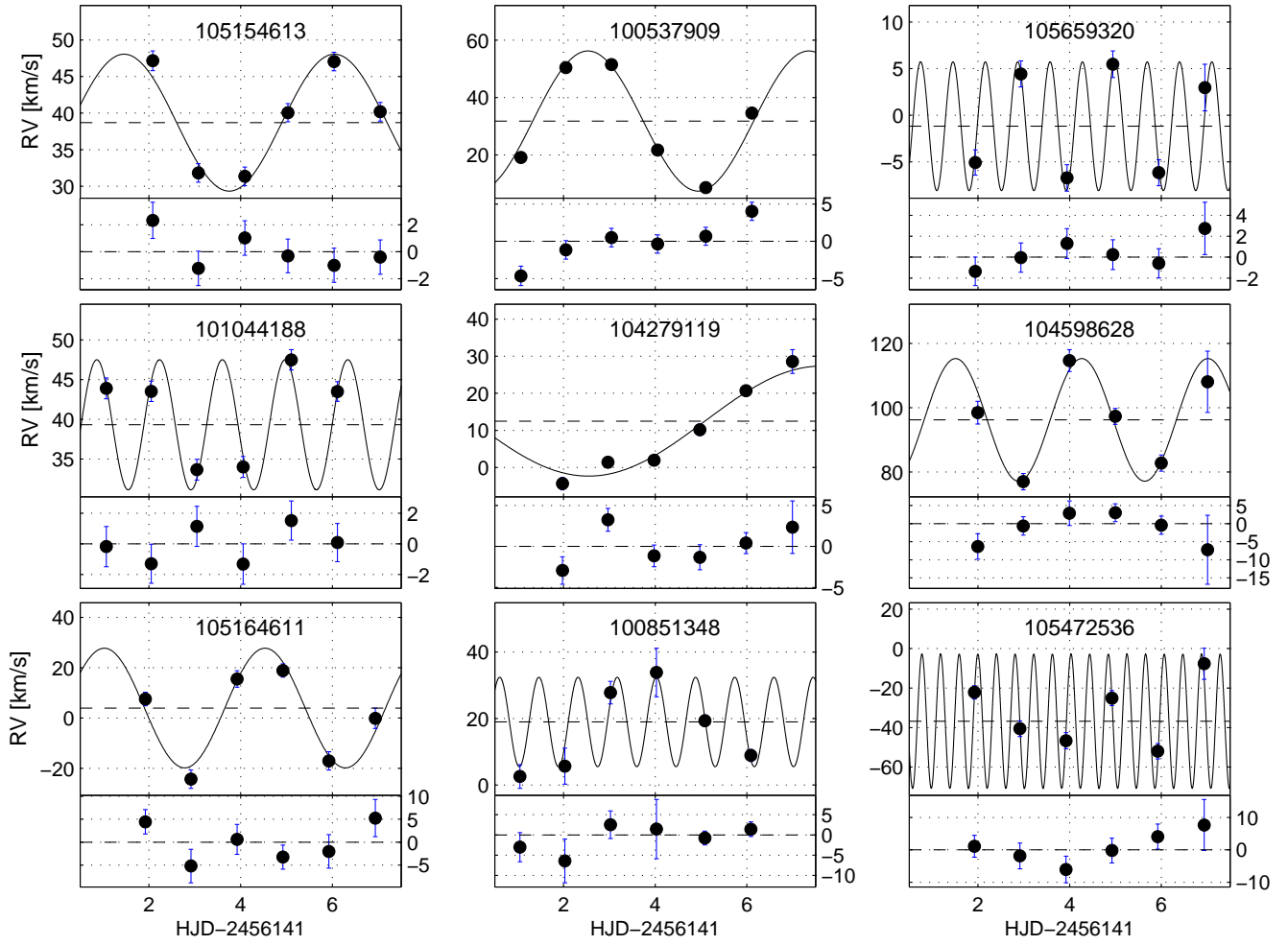


Fig. 12. Continued.

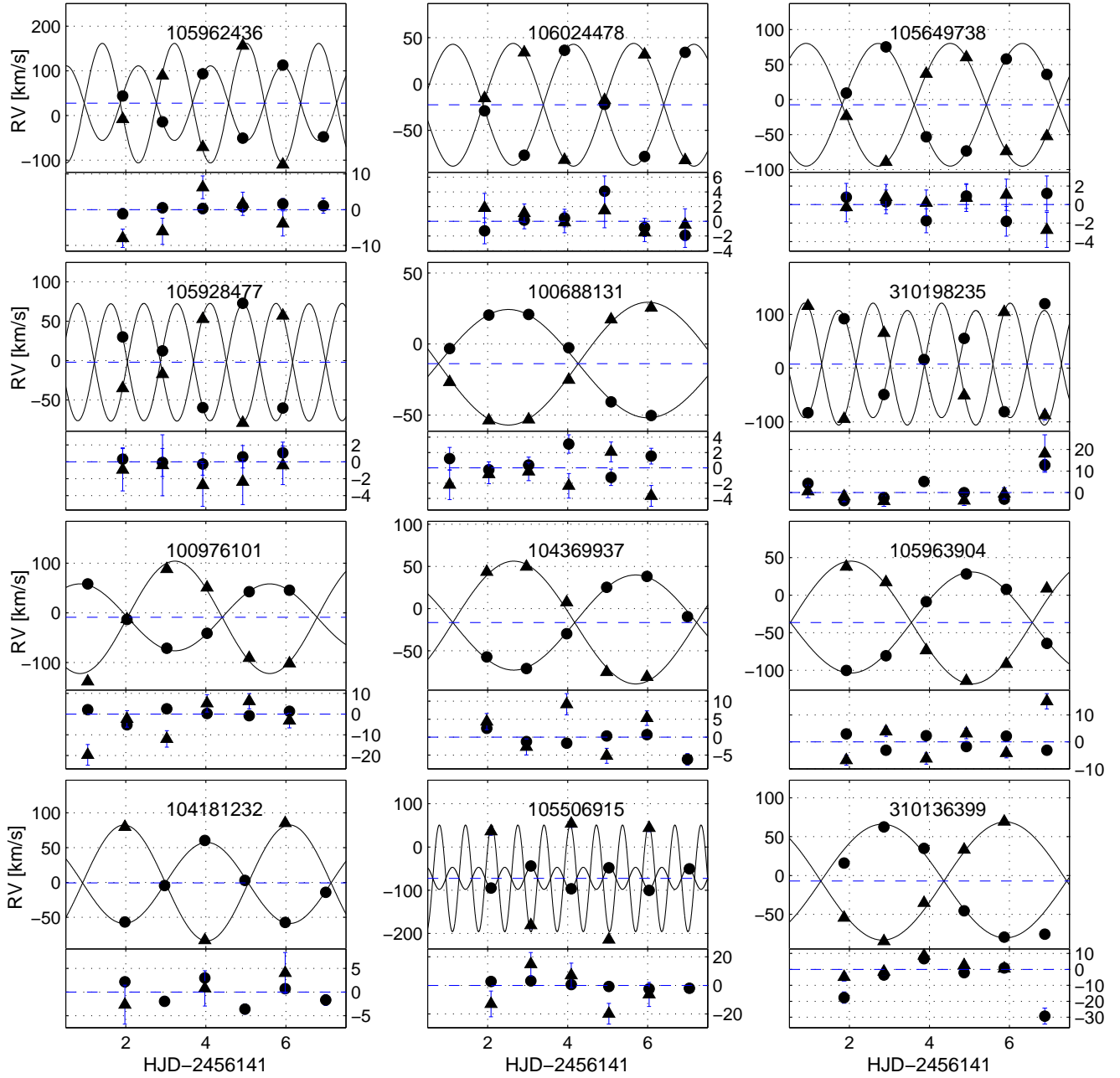


Fig. 13. AAOmega RVs and the best-fit Keplerian models (solid lines) of the confirmed BEER SB2s listed in Table 7. Primary RVs are marked with circles and secondary RVs are marked with triangles.

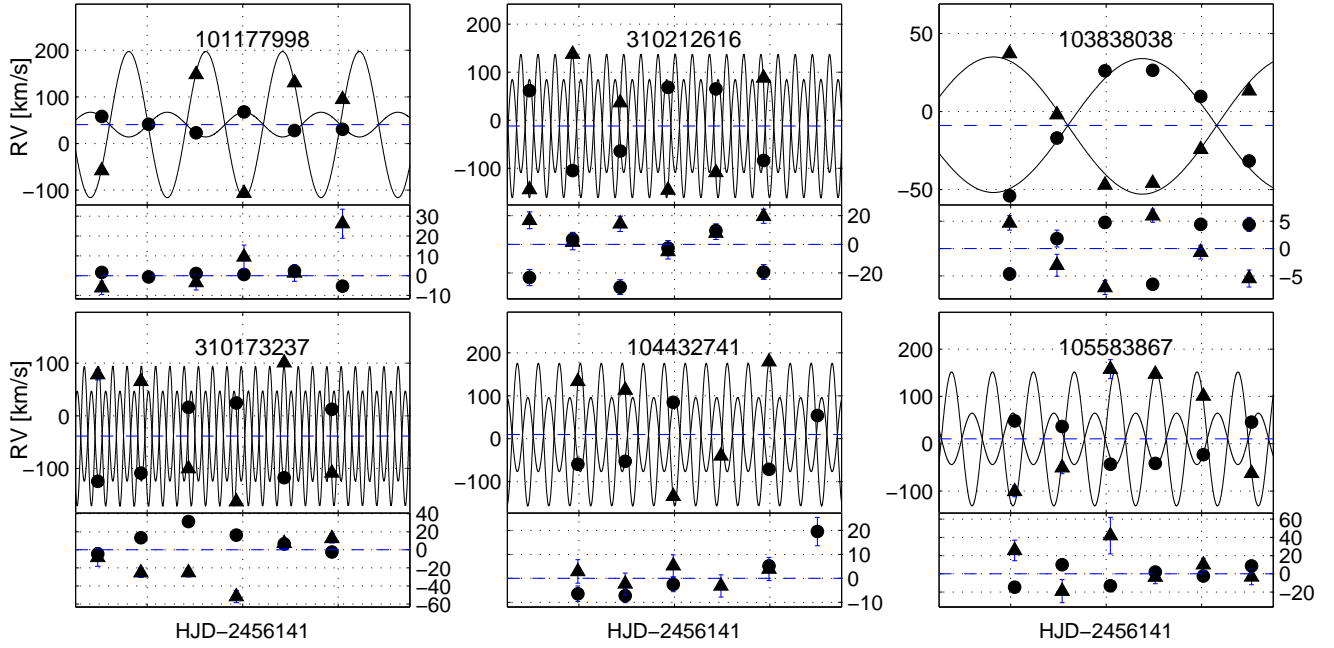


Fig. 13. Continued.

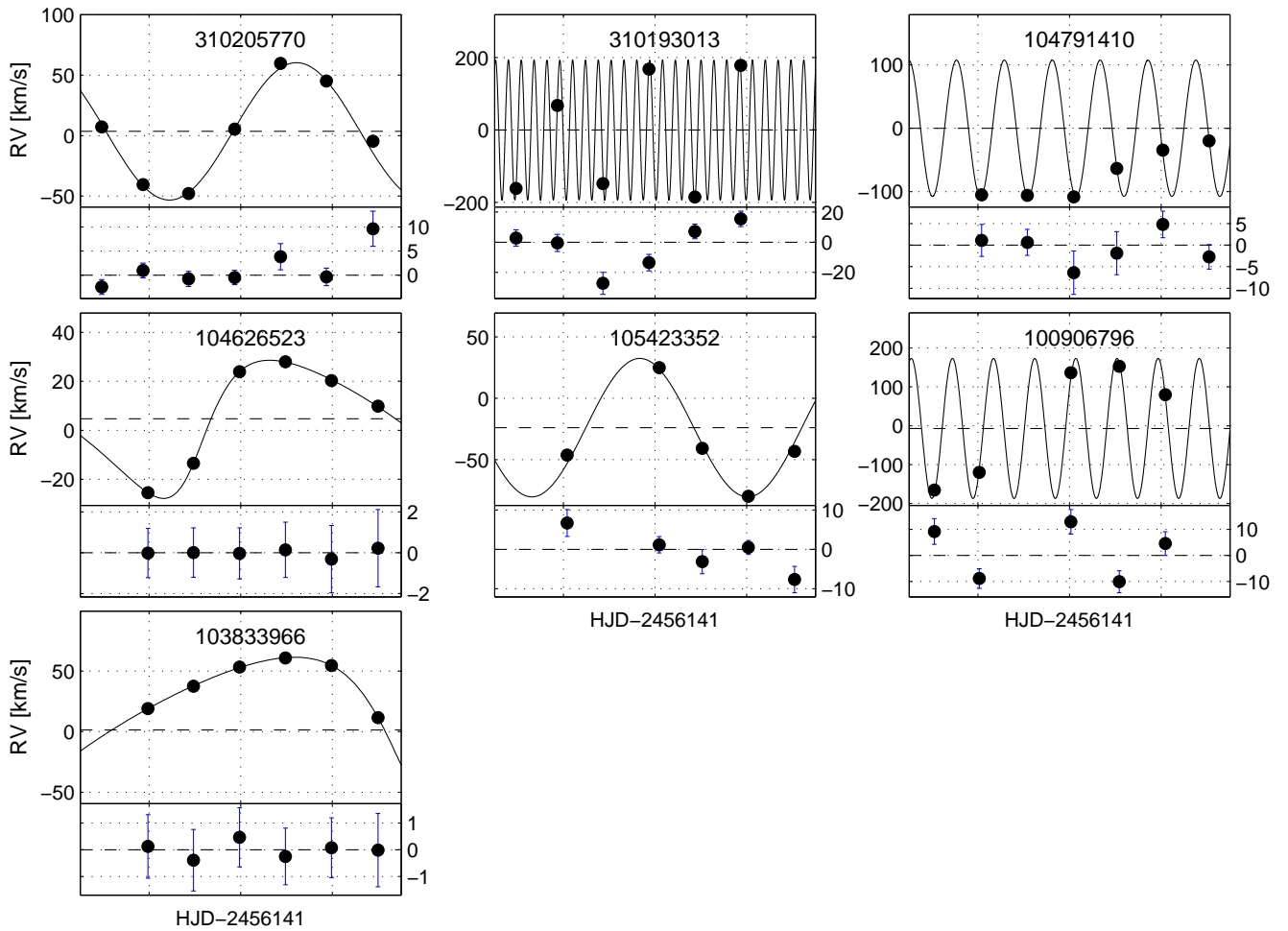


Fig. 14. AAOmega RVs (black circles) and the best-fit Keplerian models (solid lines) of the variable components in the confirmed BEER diluted binaries listed in Table 8.

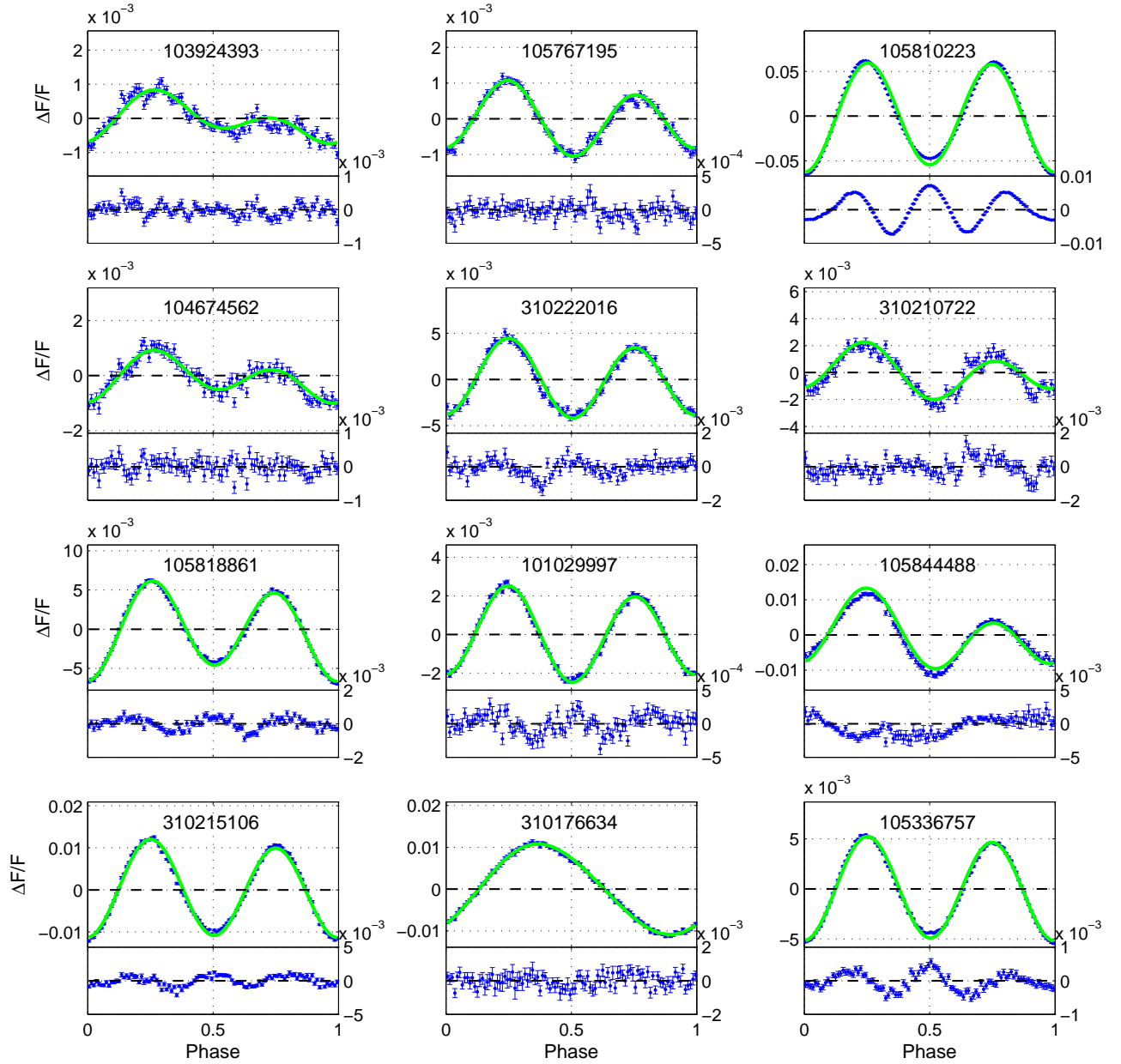


Fig. 15. Phase-folded and binned lightcurves (blue) and the best-fit BEER models assuming a circular orbit (green) of the 70 BEER binaries confirmed by AAOmega.

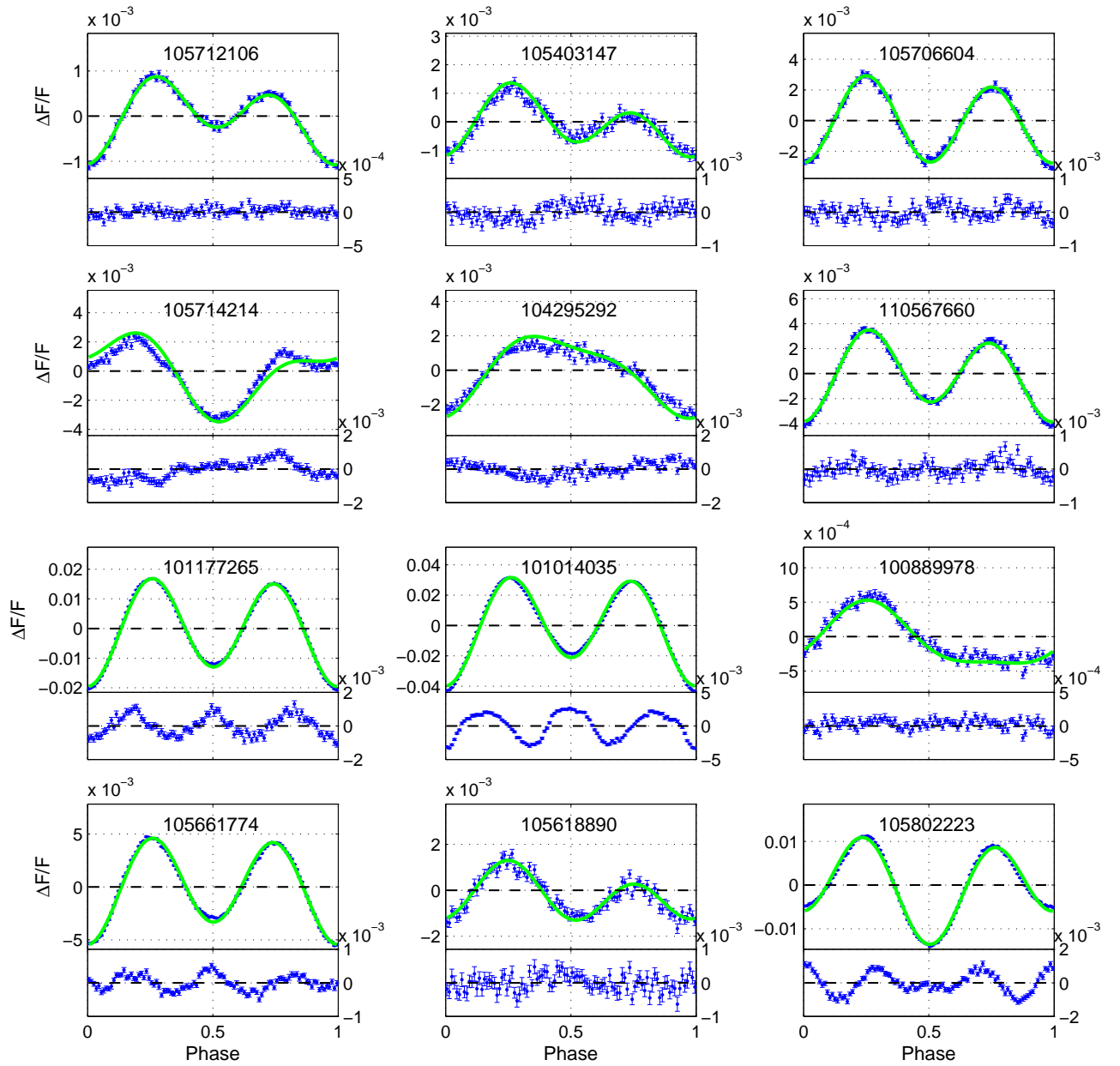


Fig. 15. Continued.

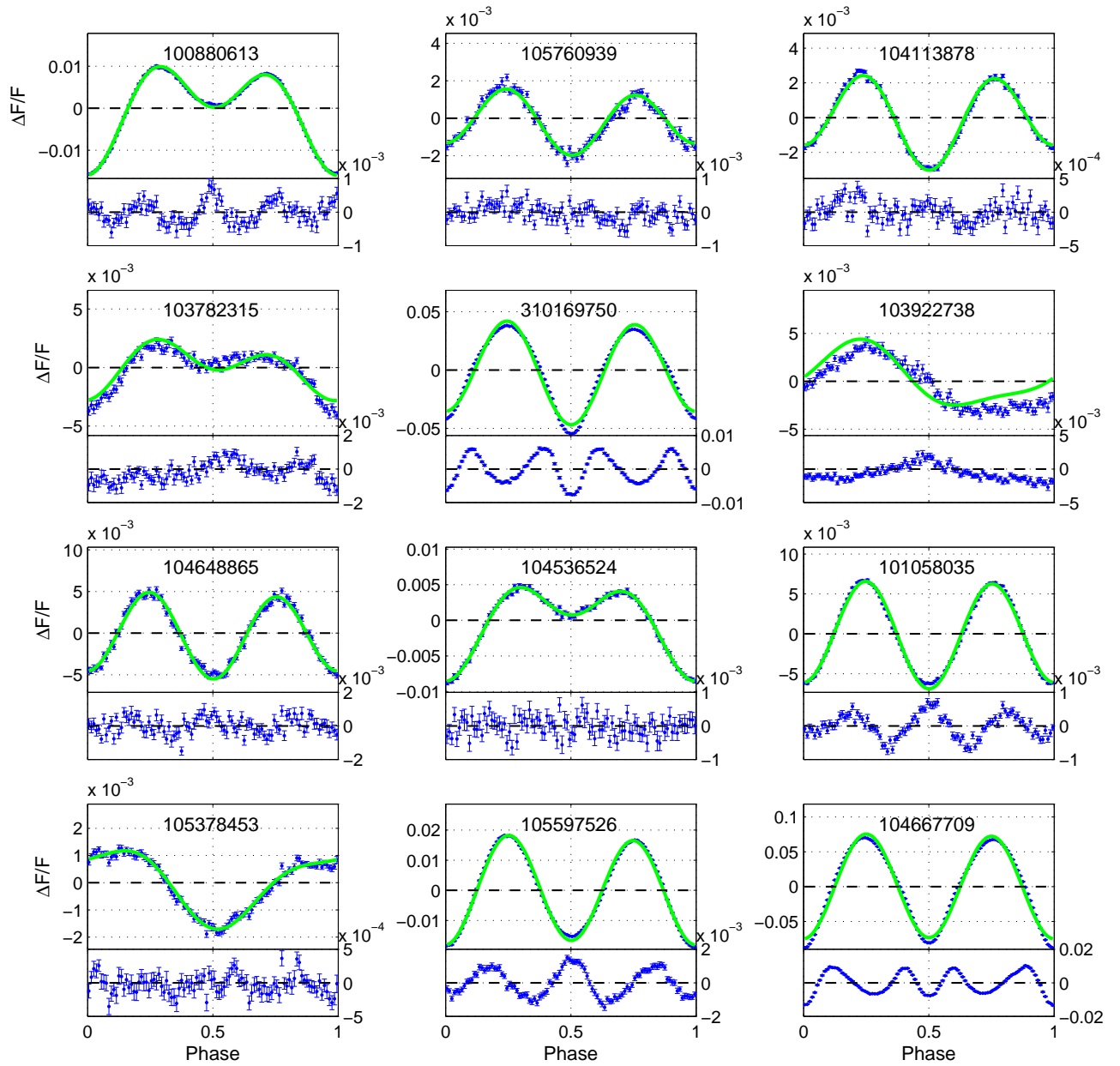


Fig. 15. Continued.

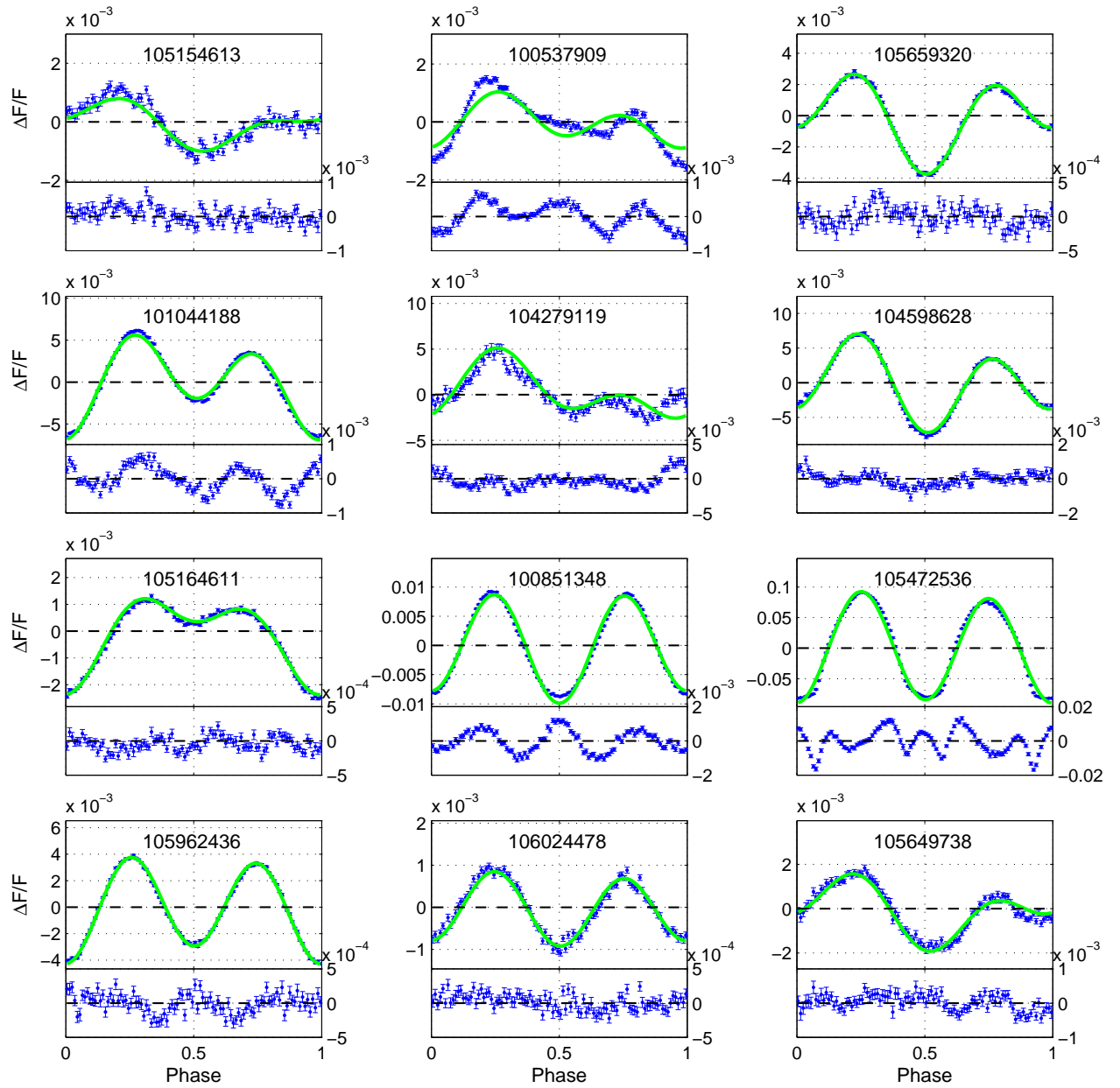


Fig. 15. Continued.

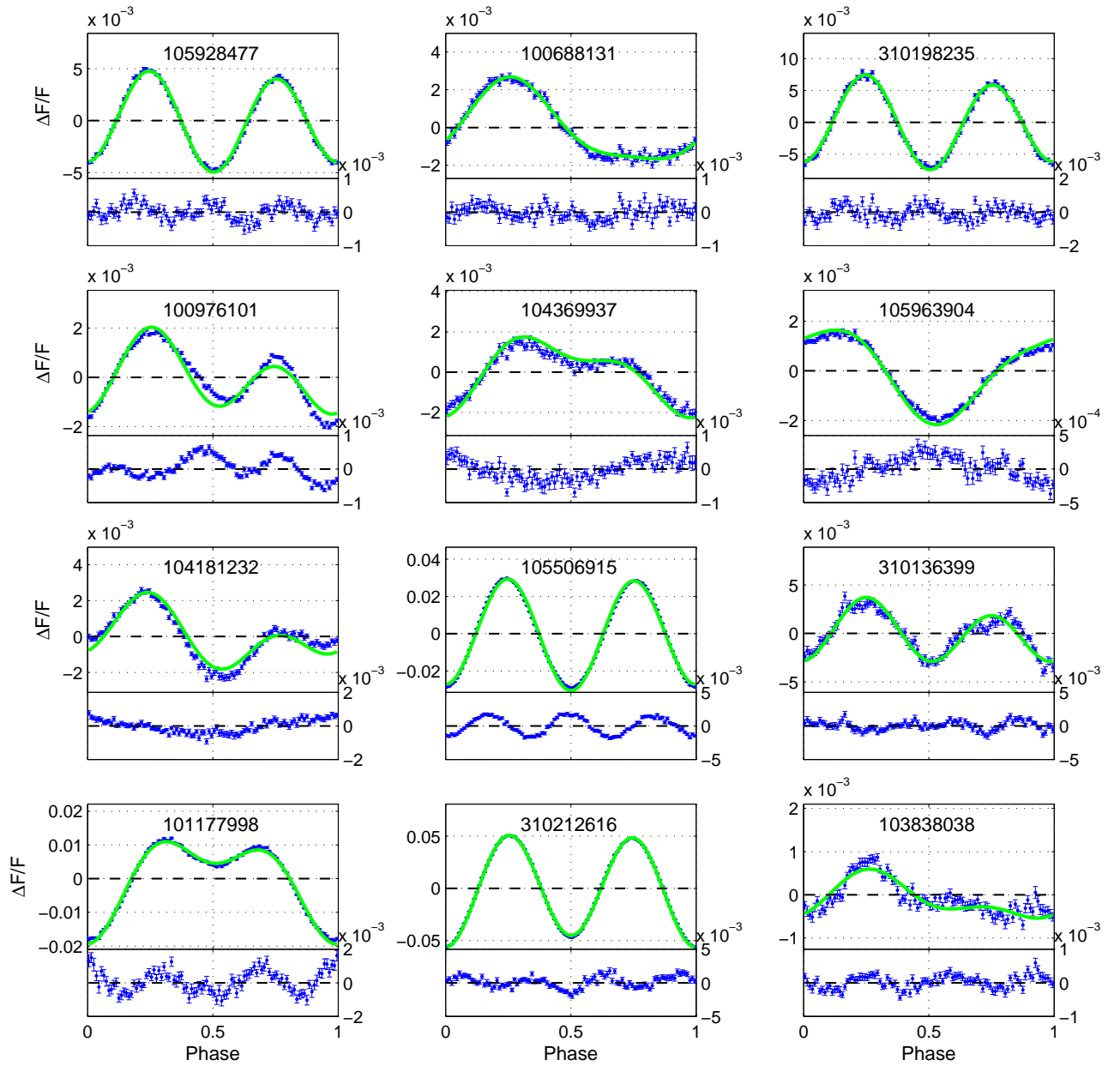


Fig. 15. Continued.

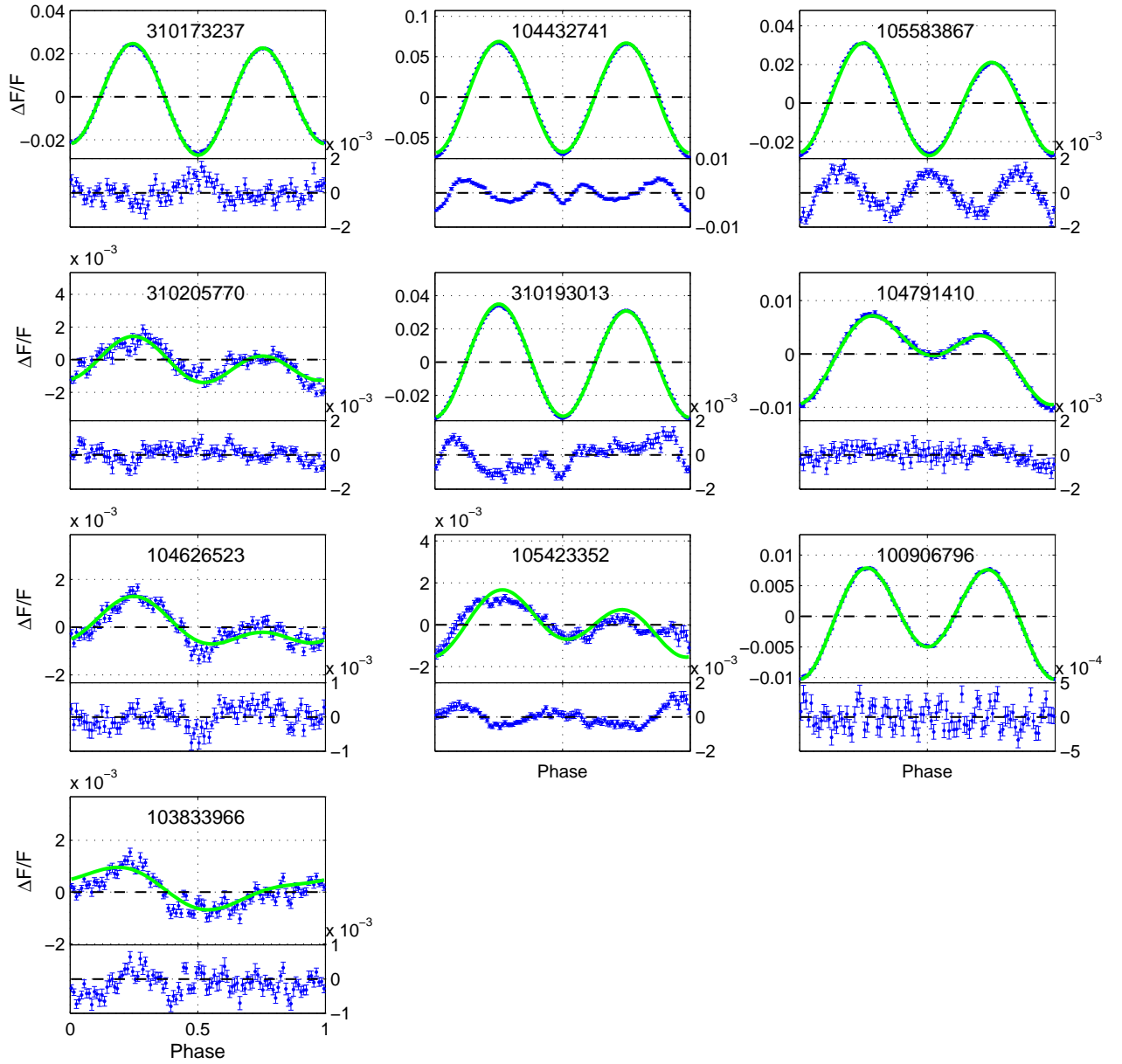


Fig. 15. Continued.